Amyloid-beta, alpha-synuclein and tau aggregated co-pathologies enhance neuropathology and neuroinflammation

Jhodi M. Webster[1, 2], William J. Stone[1], Ya-Ting Yang[1, 2], Aidan T. Miller[1], Gabrielle M. Childers[1], Nicole J. Corbin-Stein[1], Nikhita Mudium[1], Jeremy Molina[6], Woong-Jai Won[1], Ivette M. Sandoval[5], Daniel J. Tyrrell[3], Frederic P. Manfredsson[2, 5], Jeffrey H. Kordower[2,6], and Ashley S. Harms[1, 2]*

Author affiliations:

[1]University of Alabama at Birmingham, Department of Neurology, Center for Neurodegeneration and Experimental Therapeutics, Birmingham, AL

[2]Aligning Science Across Parkinson's (ASAP) Collaborative Research Network, Chevy Chase, MD, 20815, USA

[3]University of Alabama at Birmingham, Department of Pathology and Division of Molecular and Cellular Pathology, Birmingham, AL

[4]Neurodegenerative Diseases Research Unit, Biogen, Cambridge, MA

[5]Barrow Neurological Institute, Department of Translational Neuroscience; Phoenix, AZ.

[6]Arizona State University, ASU-Banner Neurodegenerative Disease Research Center, Bio-design Institute, Tempe, AZ

***Correspondence to:**

Ashley S. Harms

University of Alabama at Birmingham, 1719 6th Ave South, Birmingham, Alabama 35294

anharms@uab.edu

Running title: Co-pathologies drive neuroinflammation in disease

Keywords: co-pathologies, neuroinflammation, α-synuclein, tau, amyloid beta, T cells, microglia

Abstract

Lewy pathology due to alpha-synuclein (α-syn) inclusions is one of the major hallmarks of Parkinson's Disease (PD). β-Amyloid (Aβ) and phosphorylated-tau, pathologies usually found in Alzheimer's Disease (AD), have also been implicated in PD, with over 50% of patients exhibited the co-expression of these proteins (co-pathologies). In both AD and PD postmortem tissue, neuroinflammation – the activation of microglia and resident macrophages and the infiltration of immune cells from the periphery, including T cells and monocytes–are drivers of neurodegeneration. However, how the co-expression of these pathologies contribute to the inflammatory response and overall neurodegenerative disease phenotype remains unknown. To understand how the co-expression of pathologies drives neuropathology, we developed a novel co-pathology model by stereotaxically injecting α-syn pre-formed fibrils (PFFs) into the striatum, and AAV-double^{mut} tau virus into the entorhinal cortex, of 3-month-old J20 transgenic mice with Aβ pathology. We analyzed immune cell populations in the brain and periphery at 3 months post-induction (3MPI). At 6MPI, neuronal loss in the hippocampus and substantia nigra pars compacta were assessed along with pathological protein deposition. At 3MPI, the co-pathology mouse model begins to exhibit enhanced pathology load in the cortex and hippocampus. There was a robust neuroinflammatory response in interconnected brain regions, including increased microglial cell number, changes in microglial activation markers, and infiltration of T cells. This was synergistic in the co-pathology model, compared to the individual models, supporting the hypothesis that these collectively may drive the progression of disease.

Introduction

In addition to the progressive loss of neurons and brain atrophy, neurodegenerative diseases share the common feature of pathogenic protein accumulation. These include α-synuclein (α-syn) inclusions found in Lewy bodies and Lewy neurites in Parkinson disease (PD), extracellular amyloid-βeta (Aβ) plaques and phosphorylated-tau tangles in the form of intracellular neurofibrillary tangles (NFT) in Alzheimer's disease (AD) [1-3]. Although these proteins have been classically found in their respective diseases, there has been evidence for the overlap of pathology and symptoms. The presence of these AD-related pathologies, found in 50-80% of PD brains [4-11], has been a significant contributor to exacerbated disease progression and dementia onset in patients with PD [9, 12]. Similarly, α-syn inclusions have been found in the brains of AD patients. The co-expression of these pathologies has been linked to worsened cognitive decline and higher rate of mortality in diseased patients [13, 14]. These clinical results suggest synergism between α-syn, tau and Aβ, however the disease-progressing mechanisms of this co-expression remain unknown.

Neuroinflammation, including the activation of resident immune cells in the brain and the infiltration of lymphocytes and monocytes from the periphery, has been highlighted as a major driver of neuronal loss and disease progression. CD4 and CD8 T cells are found in the brains and cerebrospinal fluid (CSF)[15] of AD [16-19] and PD [20-22], and dementia with Lewy body (DLB) patients along with activation of myeloid cells. This includes changes in activation states of resident microglia, macrophages and an influx of infiltrating monocytes. Antigen presentation between myeloid cells and lymphocytes is an important process in eliciting an adaptive immune response and eliminating pathogens. In neurodegenerative diseases such as PD, single nucleotide polymorphisms in human leukocyte antigen (HLA), also known as major histocompatibility

complexes I and II (MHCI and MHCII) in mice, are associated with increased risk of disease indicating a key role in disease pathogenesis and/or progression [23, 24]. These responses have been recapitulated in animal models, where antigen presentation by MHCII to an increased population of T cells in the substantia nigra pars compacta, is crucial for neuronal death in a viral α-syn overexpression model [25]. The combined innate and adaptive immune response contributes to the release of pro-inflammatory cytokines, promoting the damage and eventual death of neurons.

Previously published co-pathology mouse models have confirmed potential synergistic interactions with co-expression of these pathologies. DLB-AD mice, a cross of 3xTg AD mice with α-syn A53T mice yielded the creation of the first triple pathogenic model [26]. This model was able to highlight that α-syn, tau and Aβ pathologies synergize to promote the aggregation of each other and accelerated cognitive decline. However, there were no differences in microglia or astrocyte reactivity compared to individual pathology controls. PD-AD mice (mouse α-syn PFF in 5xFAD mice) induced increasing p-tau and Aβ plaque burden [27]. Using AD-derived tau along with α-syn PFFs, tau burden and spreading was significantly increased to single pathology animals [28]. In these animal models, however, inflammation in the presence of the pathologies was not fully assessed. As such, it remains unknown how these co-pathologies promote the immune cell activation leading to the neurodegeneration and sustained aggregated protein pathology seen in patient samples.

To determine whether α-syn, tau and Aβ as co-pathologies promote neuroinflammation, protein pathology load and neuronal loss, we injected an AAV-double mutant tau (AAV-dbl^{mut} tau) virus and α-syn mouse pre-formed fibrils (mPFFs) into the entorhinal cortex and striatum respectively of 3-month-old J20 transgenic mice, that overexpress human mutant amyloid protein precursor (APP) resulting in Aβ plaques in the cortex and hippocampus. With this co-pathology

model, we assessed for both innate and adaptive immune responses, as well as protein pathology. Finally, we studied how these proteins synergistically affected neurodegeneration in the substantia nigra pars compacta and the regions of the hippocampus. Utilizing this co-pathology mouse model, we found the presence of co-pathologies not only began to enhance abnormal protein deposition compared to individual pathology controls, but also neurodegeneration in the hippocampus and innate and adaptive neuroinflammatory responses. Results from these studies suggest synergistic mechanisms underlying neurodegeneration and the onset of cognitive impairments in neurodegenerative diseases.

Materials and Methods

Mice

The mouse strain used for this research project, B6J.Cg-*Zbtb20*$^{Tg(PDGFB\text{-}APPSwInd)20Lms}$/Mmjax, (RRID:MMRRC_034836-JAX), was obtained from the Mutant Mouse Resource and Research Center (MMRRC) at The Jackson Laboratory, an NIH-funded strain repository, and was donated to the MMRRC by Lennart Mucke, Ph.D., Gladstone Institute of Neurological Disease. Age and sex-matched non-transgenic littermates (NTG, C57BL/6J background) were used for sham and single pathology induction. For all experiments presented, both male and female mice were used. All research conducted on animals was approved by the Institutional Animal Care and Use Committee at the University of Alabama at Birmingham and methods followed the Animal Research: Reporting of *In vivo* Experiments (ARRIVE) 2.0 guidelines (arriveguidelines.org).

Fibril and viral vector generation

Mouse α-synuclein pre-formed fibrils

α-syn mouse pre formed fibrils (PFFs) were generated and purified from mouse α-synuclein from the Volpicelli-Daley lab at the University of Alabama at Birmingham according to previously published protocols [29, 30]. Briefly, mouse PFFs were thawed and aliquoted into 25uL (5mg/mL) and transferred to polystyrene sonication tubes. Tubes containing PFFs were then transferred to a Q700 Sonicator water reservoir once the water was at 10C. Fibrils were sonicated for 15 minutes, with pulse on and off durations, at a power of approximately 110 watts per pulse. After sonication, tubes are quickly spun down and 1uL of sonicated PFFs transferred into an Eppendorf tube in 1X PBS, for a final volume of 500uL. 5uL of this solution is sent for dynamic light scattering analysis to check for PFF fragmentation of around 50nm after sonication.

AAV9-double mutant tau virus

Recombinant adeno-associated virus capsid 9 (AAV9) vectors were generated as described in prior studies, engineered to express human mutant tau variants (P301L/S320F), driven by the hybrid chicken β-actin promoter[31]. Vector concentrations were assessed using qPCR and expressed as viral genomes per mL (vg/mL)

Stereotaxic injections

Mice aged 12-14 weeks old were deeply anesthetized using an isofluorane vaporizing instrument (UAB Animal Resource Program) and immobilized to a stereotaxic frame (Stoelting) on top of a heating pad to ensure appropriate internal body temperature is maintained. 26s/2"/2 10μL Hamilton syringes along with an automatic injecting system (Stoelting) are used to unilaterally (immunohistochemistry, DAB and fluorescence) or bilaterally (behavior, flow cytometry) inject

2uL of mouse α-syn PFFs (5μg/mL), mouse α-syn monomer (5μg/mL), AAV9-dbl^{mut} tau virus (3.2E12vg/mL) or AAV9-GFP (3.2E12vg/mL). PFFs or monomer control were injected into the dorsal lateral striatum based on bregma (AP +0.5mm, ML +/-2.0mm and DV -3.0mm from the dura) AAV9-dbl^{mut} tau or AAV9-eGFP viruses were injected into the entorhinal cortex (AP -3.5mm, ML +/-3.9mm and DV -4.2mm from dura). Injection needle was left in the injection site for an additional 2 minutes following completion and then slowly retracted from the site over the course of another 2 minutes. All surgical protocols and post-surgery aftercare methods were followed and approved by the Institutional Animal Care and Use Committee at the University of Alabama at Birmingham.

To induce the co-pathology model, 3-month-old J20 transgenic mice were injected with mouse α-syn PFFs into the striatum and AAV9-dbl^{mut} tau virus into the entorhinal cortex. For sham surgery, non-transgenic littermates were injected with mouse α-syn monomer and AAV9-eGFP into the striatum and entorhinal cortex, respectively.

To induce single pathology controls, non-transgenic mice were injected with mouse α-syn PFFs into the dorsal lateral striatum for α-syn models and AAV9-dbl^{mut} tau virus into the entorhinal cortex for tau models. α-syn monomer into the striatum and AAV9-GFP were injected into the dorsal lateral striatum and entorhinal cortex, respectively, of non-transgenic mice as controls. J20 transgenic mice were used as the Aβ single pathology mice, compared to un-injected non-transgenic littermates.

Tissue preparation and processing

At 3 months post-induction (3MPI) and 6 months post-induction (6MPI) of the co-pathology model and single-color controls, mice were anesthetized using isofluorane and transcardially perfused with 0.01M phosphate-buffered saline (PBS, pH = 7.4) and fixed with 4% paraformaldehyde (PFA in PBS, pH = 7.4). Brains were then dissected and incubated in 4% PFA for 2 hours at room temperature. After fixation, brains were placed in 30% sucrose in PBS for 3 days until brains were fully saturated. Brains were then frozen on dry ice and cryosectioned coronally at 40μm on a sliding microtome (Thermo Scientific Micron HM 450). Sliced brain tissue was then stored in a 50% glycerol/PBS solution at -20ºC.

Immunofluorescent immunohistochemistry

Free-floating 40-μm thick sections were washed in 0.01M tris-buffered saline solution (TBS, pH 7.4) prior to an antigen retrieval process with a solution of 10mM sodium citrate and 0.05% Tween-20 in TBS. Sections were then incubated in 5% blocking serum at room temperature before being incubated overnight in the following primary antibody solutions (TBST, 1% serum): anti-CD4 (clone RM4-5, ThermoFisher), anti-CD8 (clone 4SM15, eBioscience) and anti-Iba1 (WACO). On the following day, sections were washed in TBS with .1% Triton-100 and incubated in fluorescent conjugated antibody in the dark for 2 hours at room temperature. Sections were then washed in TBST and mounted on microscope slides for analysis. Slides were imaged at 20X on a Nikon A1 Laser Scanning Confocal microscope.

DAB immunohistochemistry

Free-floating 40-μm thick sections were washed in 0.01M tris-buffered saline solution (TBS, pH 7.4) prior to being quenched with 3% hydrogen peroxide in TBS for 5 minutes. Next, sections

underwent an antigen retrieval process with a solution of 10mM sodium citrate and 0.05% Tween-20 in TBS for 30 minutes at 37°C. Following this, sections were blocked in a 5% goat or donkey serum solution for at least 1 hour at room temperature and then incubated overnight at 4°C with the following antibodies in 1% serum solution: anti-CD3 (clone 17A2, eBioscience), anti-tyrosine hydroxylase (clone: EP1536Y, Abcam), anti-alpha synuclein, phosphor-serine 129 (pSer129, close EP1536Y, Abcam), anti-AT8 (clone MN1020, ThermoFisher), anti-Aβ(clone D54D2, Cell Signaling) and anti-NeuN (clone EPR12763, Abcam). Sections were then incubated with a biotinylated secondary antibody (1:1000, Vector Labs) in a 1% serum in TBST solution. After incubation, sections were washed with TBS and incubated in the Vectastain ABC Reagent (Vector Labs) for 30 minutes at RT prior to development with the Vectastain diaminobenzidine DAB Kit (SK-4199, Vector Labs) according to the manufacturer's protocol. Sections were then mounted onto plus-coated slides and dehydrated with a gradient of ethanol solutions (70%-100%) followed by Citrisolv. Slides were them coverslipped with Permount Mounting Media (Electron Microscopy Sciences). Slides were then images at 10X and 20X on a Zeiss Imager M2 brightfield microscope (MBF Biosciences).

Brain single cell isolation and flow cytometry

At 3MPI, co-pathology and single pathology mice were anesthetized and transcardially perfused with 0.01M PBS (pH 7.4). Briefly, brain tissue was removed and the striata (STR), hippocampi (HIP), cortices (CTX), midbrains (MB) and entorhinal cortices (ENT) dissected. Tissue was then digested with 1 mg/mL Collagenase IV (Sigma) diluted in RPMI 1640 (1X, Gibco). Following enzyme digestion, tissue was then filtered and smashed through a 70μm filter using a syringe plunger and mononuclear cells isolated out using a 30/70% Percoll gradient (GE).

For cell staining, isolated brain cells were blocked with anti-Fcγ receptor (1:100, Biosciences). Following this, cell surface markers were labelled with the following, fluorescent-conjugated antibodies against CD45 (clone 30-F11, eBioscience), CD11b (clone M1/70, BioLegend), MHCII (M5/114.15.2, BioLegend), Ly6C (clone HK 1.4, BioLegend), TCRβ (clone H57-597, Biolegend), CD4 (GK1.5, BioLegend), CD8a (clone 53-6.7, BioLegend). CD69 (clone H1.2F3, BioLegend), PD-1 (clone 29F.1A12, BioLegend), B220 (clone RA3-6B2, BD Biosciences), CD44 (clone IM7, Biolegend), CXCR3 (clone 173, BioLegend), CD62L (clone MEL-14, BioLegend), CD103 (clone 2E7, BioLegend), CD25 (clone PC61.5, Invitrogen), TLR2 (clone CB225, BD Biosciences), Ki67 (clone 16A8, BioLegend), P2RY12 (clone S16007D, BioLegend), CX3CR1 (clone SA011F11, BioLegend), CD68 (clone FA-11, BioLegend). A fixable viability dye was used to distinguish live cells, per the manufacturer's protocol Aqua-LIVE/DEAD Stain Kit (Invitrogen). As single-color compensation controls, isolated splenocytes or UltraComp eBeads™ (Invitrogen) were used. To analyze and run samples, a BD Symphony (BD Biosciences) or Spectral Enabled Symphony flow cytometer were used at the UAB Flow Cytometry and Single Cell Core Facility. Mean cell counts, percentages and mean fluorescent intensity were measured and analyzed using FlowJo (Tree Star) software.

Mouse brain lysate preparation

Brain tissue was micro dissected, snap frozen in super-cooled bath of 2-methylbutane with dry ice, and stored at -80°C. Tissue lysates were homogenized with a tissue grinder using 20% weight/volume lysis buffer (50 mmol/L Tris-HCl pH 7.4, 175 mmol/L NaCl, 5 mmol/L EDTA) supplemented with protease and phosphatase inhibitors and sonicated for 10 sec on ice. After

addition of Triton X-100 to a final concentration of 1% volume/volume, samples were incubated on ice for 30 minutes and centrifuged at 15,000 xg for 60 min at 4°C. The supernatant was saved as the Triton X-100 soluble fraction. The pellet was resuspended in lysis buffer with 2% SDS, sonicated for 10 sec, and centrifuged for 10 minutes at 15,000 xg. The resulting supernatant was reserved as the Triton X-100 insoluble fraction. Protein concentration was determined by the bicinchoninic acid assay (Pierce Cat# 23225).

Amyloid β (Aβ) 1-40 and 1-42 ELISA

A total of 20 µg brain lysate was used to measure concentrations of Aβ 1-40 and 1-42 with the human Amyloid beta (aa1-40) Quantikine ELISA (R&D Systems Cat# DAB140B) and human Amyloid beta (aa1-42) Quantikine ELISA (R&D Systems Cat# DAB142) kits, respectively. Colorimetric signal was measured using the SpectraMax iD3 (Molecular Devices). Results reported as the ratio of Aβ 1-42/1-40.

Dot blotting

Samples were dotted onto a nitrocellulose membrane and allowed to dry for 15 minutes before blocking with 5% non-fat milk. Blots were then incubated in primary antibody for 1.5 hours with Tau (1:1000, Cell Signaling Technology Cat# 46687, RRID:AB_2783844), PHF-tau (1:1000, P. Davies Albert Einstein College of Medicine; New York; USA Cat# PHF1, RRID:AB_2315150), or Alpha-synuclein aggregate (1:1000, Abcam Cat# ab209538, RRID:AB_2714215). Following 3 x 10 minute washes in Tris-buffered saline with 0.1% Tween 20 (TBST), blots were incubated with HRP conjugated goat anti-mouse (1:2000, Jackson ImmunoResearch Labs Cat# 115-035-146, RRID:AB_2307392) or goat anti-rabbit (1:2000, Jackson ImmunoResearch Labs Cat# 111-

035-144, RRID:AB_2307391) for 1 hour. Washes were repeated and blots were visualized using Clarity ECL (Bio-Rad) on a ChemiDoc MP imaging system (Bio-Rad). Dot intensity was measured, and background subtracted using ImageJ v1.54f.

Quantification and Statistical Analysis

Unbiased Stereology of the hippocampus and substantia nigra pars compacta

In order to quantify neuronal cell loss, an unbiased stereology protocol was used. TH and NeuN-DAB stained (see 'DAB Immunohistochemistry' section) SNpc and hippocampal tissue sections, respectively, were imaged and analyzed with a Zeiss Axio Imager M2 microscope (MBF Biosciences) and the Cavalieri stereology probe used to count cells, with a section thickness of 25µm to account for dehydration of sections. To quantify NeuN+ neurons in the hippocampus, contours were drawn around the five to seven sections, focusing on the CA1 and CA3 regions. To quantify Th+ neurons in the SNpc, contours were drawn around both sides of the nigra, in four to five sections. Similar contours were drawn in the nigra to quantify α-syn+ neurons. For stereological counting, the grid size used for the hippocampus was 130x130 and the counting frame was 40µmx40µm. In the SNpc, the grid size and counting frame were, 100x100 and 50µmx50µm, respectively.

Statistical Analysis

All graphs and subsequent statistical tests were generated using Prism software (GraphPad) or Jupyter notebook as described [32]. Flow cytometry experiments used ten to twelve independent samples with two brain regions pooled per sample, for a final number of five to six per group for

experiments. Data were analyzed using an unpaired student's t-test or a one-way ANOVA. Graphs within display the mean +/- SEM. For unbiased stereology, estimated populations were generated and a one-way ANOVA was used to determine the significance between groups. *$p<0.05$, **$p<0.01$, ***$p<0.0005$, ****$p<0.0001$.

Data availability

The authors affirm that the findings within the manuscript are supported by the data therein. Additional information and datasets are available upon request from the corresponding author.

Results

The accumulation of Aβ plaques, intracellular tau tangles and p-α-syn inclusions are promoted within varying brain regions in the co-pathology mouse model

To generate a co-pathology model that included the presence of Aβ, α-syn, and tau co-pathologies, 12-14 week old J20 transgenic were stereotaxically injected with 5μg of mouse α-synuclein (α-syn) pre-formed fibrils (PFFs) to produce α-syn inclusions in the dorsal lateral striatum (STR), cortex (CTX), and substantia nigra (SNpc) , and 2μL of an adeno-associated virus (AAV) overexpressing human mutant tau (S320F/P301L mutations), AAV-dbl^{mut} tau into the entorhinal cortex (ENT) (Figure 1a). Age-matched non-transgenic (NTG) littermates were injected with either 5μg of α-syn PFFs into the striatum or AAV-dbl^{mut} tau into the entorhinal cortex to induce PFF and tau single pathology controls. (Figure 1a). Age-matched, J20 mice were used as Aβ single pathology controls. At both 3 (Figure 1) and 6 months post-induction (MPI) (Supplementary figure 1), Aβ plaques and AT-8-positive neurons were immunolabeled via diaminobenzidine (DAB) immunohistochemistry, and shown to be present in the hippocampus (HIP) and CTX of co-

pathology mice (Figure 1c,m). α-syn inclusions were found within the SNpc, amygdala (AMG) and CTX at 3MPI (Figure 1b), with this Lewy-like pathology also seen within the HIP at 3MPI (Figure 1b). Similar pathology is seen at 6MPI with α-syn pathology seen across the SNpc, CTX, STR and AMG (Supplementary Figure 2b). Aβ and tau were labeled across the HIP and CTX (Supplementary Figure 1a,c). To determine how these pathologies may be influencing the aggregation and accumulation of each other, we investigated the effect of a co-pathology on the expression of α-syn, tau and Aβ. At 3MPI the HIP, CTX, MB and STR were isolated from PFF mice and the HIP and CTX from J20 and Tau single pathology mice for dot blot analysis. Triton X-100 soluble and insoluble fractions were prepared and isolated. Utilizing dot blots for aggregated α-syn, total tau and phosphorylated tau (pTau) in lysates from 3MPI, results show early changes in α-syn and Aβ load in the CTX and HIP of the co-pathology model mice compared to PFF single pathology brains (Figure 1d,f,g). Similarly, increases in total tau and pTau were seen in the HIP and CTX of co-pathology brains (Figure 1e-l). Lastly, enzyme linked immunosorbent assay (ELISA) probing from human Aβ1-40 and 1-42 showed slight changes in Aβ42/40 ratio in the HIP, but not CTX of co-pathology brains compared to J20 single pathology controls (Figure 1o). These results indicate enhanced pathology load and aggregation of other proteins in a co-pathology environment beginning at 3MPI.

Neuronal loss is driven by the co-expression of abnormal aggregated proteins

Neurodegeneration, including changes in synaptic density and the subsequent death of neurons, occurs upstream of the severe onset of symptoms associated with disease – such as cognitive and motor impairments [33-36]. Given the involvement of α-syn, tau and Aβ in neurodegenerative disease, we next examined how co-expression would impact neuronal survival and integrity. Using

unbiased stereology at 6 MPI, we found enhanced neurodegeneration of NeuN+ neurons in the CA1 region of the hippocampus in the co-pathology mice compared to tau, J20 or α-syn PFFs alone (Figures 3a-b). Within the CA3, co-pathology mice showed significant loss compared to single Tau and PFF controls (Figure 3c). In the SNpc at 6 MPI, where α-syn pathology is present (Supplementary Figure 1), TH positive neuron loss in the co-pathology model is significantly enhanced compared to that in the J20 animals. However, in comparison to tau and α-syn PFF mice (Figure 2d,e) the presence of co-pathologies did not enhance TH positive loss (Figures 3d,e). Together, these results highlight that the presence of co-pathologies enhances neurodegeneration in the hippocampus, an area with enhanced protein pathology.

Co-pathologies drive an innate immune response, with brain-region specific changes in microglia

Given that Aβ, α-syn, and tau pathologies are all individually associated with microglia activation and infiltration of peripheral myeloid cells in *in vivo* models [37-39], we aimed to investigate the role of co-pathologies in enhancing innate immune responses in the CNS. To induce co-pathology, 12–14-week-old J20 transgenic were stereotaxically injected with 5μg of mouse α-syn PFFs in the dorsal lateral striatum and 2μL of AAV-dbl^{mut} tau into the entorhinal cortex (Figure 3a). J20 mice, NTG mice injected with 5μg of mouse α-syn PFFs, or NTG mice injected with 2μL of AAV-dbl^{mut} tau were utilized as single pathology controls (Figure 3a). At 3MPI, brain regions were dissected from co-pathology and single pathology controls for mononuclear cell isolation and flow cytometry. Utilizing flow cytometry, gating (Supplementary figure 2) for markers for proliferation and activation of microglia, including Ki67, MHCII, TLR2, P2RY12 (a key homeostatic marker that with reduced expression is associated with the transition to pro-inflammatory microglia [40,

41]) and CD68, were used to identify changes in microglia number in co-pathology conditions. The absolute number of microglia were increased in the HIP, CTX and ENT (Figure 3) as well as in the striatum, but not in the midbrain (Figure 4) indicating active microgliosis. Infiltrating monocytes were also increased across brain regions, with exception of the ENT (Figure 3k,l). In the HIP and CTX, there is an almost 3-fold increase in the number of TLR2+ microglia when compared to J20 and tau single pathology controls (Figure 3e,i)). P2RY12loMHCII+CD68+ activated, phagocytosing microglia were also increased in all brain regions compared to single pathology controls (Figure 3, Figure 4), with 1-to3-fold increases depending on brain region, indicating an active pro-inflammatory and phagocytic response (Supplementary Figure 3). Using fluorescent IHC, we immunolabeled Iba1, a marker used to visualize morphology of both homeostatic and activated microglia, in single pathology and co-pathology brains. PFF brains, specifically in the CTX (Figure 3f), MB and STR (Figure 4b,f) show more ramified processes with smaller cell bodies while co-pathology brains exhibited less ramified processes and were more ameboid in shape, confirming the changes in phenotype of these cells in response to pathologies. Overall, these results indicate that co-pathologies promote morphological changes in microglia, translating to a more activated state, likely in response to increased protein pathology load.

Using a recently developed analysis pipeline for high dimensional immune cell characterization [32], spectral flow cytometry data were processed with the Scanpy package (v. 1.10.3) in Python (v. 3.11.9), batch correction was performed via ComBat, dimensionality reduction using principal component analysis (PCA), and visualization with uniform manifold approximation and projection (UMAP) (Figure 5b). Clustering of data was conducted using the Leiden algorithm [42], followed by statistical analysis. This approach identified four distinct microglia clusters by comparing their

responses across different brain regions in the co-pathology model based on pathology abundance. With the largest microglia cell number in the HIP and ENT compared to other brain regions (Figure 5b), all clusters were enriched in some capacity across the five brain regions. Based on relative expression in the dendrogram within each cluster (Figure 5c), microglia phenotypes were identified. Cluster 0 (with low mean expression for all markers) was enriched across the CTX, HIP, ENT, MB and STR (Figure 5d). Cluster 4 (TLR2+CD68+Ki67+CD68+), a population of microglia enriched for pro-inflammatory markers and phagocytosis) was also enriched across all regions, but was significantly increased in the STR compared to other brain regions (Figure 5d, Cluster 4). This could indicate a specific, pro-inflammatory response to α-syn pathology which was specifically found in the STR at 6MPI timepoint (Supplementary Figure 1). Cluster 1, which had proliferative and antigen presenting phenotypes (MHCII+Ki67+TLR2midP2RY12midCD68mid), was significantly decreased in the HIP and ENT compared to the CTX (Figure 5d, Cluster 1). The CTX is another region like the HIP that shows expression of more than one aggregated protein, Aβ and tau. Clusters 2 and 3, which were both transition state microglia were enriched in all brain regions, which increase in the ENT, where tau pathology is induced, for Cluster 2 and 3. These results highlight a CNS-specific response to co-pathology environment across the brain. These results also indicate differential microglial responses to protein pathologies based on expression in specific brain region.

Co-pathologies enhance an adaptive immune response via T cell infiltration into the brain

Finally, given the enhanced myeloid responses with co-pathologies and the contribution of peripheral T cells to neurodegeneration *in vivo* [20, 43], we aimed to determine if T cell responses were enhanced by co-pathologies. Following co-pathology induction with stereotaxic induction of

mPFFs into the dorsal lateral striatum and AAV-dbl^{mut} tau into the entorhinal cortex (figure 6a), T cell subsets were assessed by IHC. The presence of co-pathologies enhanced infiltration of CD3+ T cells into the HIP compared to single pathology tau and J20 brains (Figure 6b-d). With mononuclear cell isolation and spectral flow cytometry we are able to show that specific T cell populations are increased or altered with co-pathology induction, using markers for tissue resident memory (TRM) T cells (CD69, CD103), exhaustion (PD-1, when cells are less function due to chronic inflammatory response), CD44 (effector, activated cells that are antigen experienced), CD25 (inflammatory T regulatory cells), CXCR3 (chemokine receptor that is important for the migration of effector T cells to inflamed tissue) and CXCR6 (chemokine receptor that is important for retention within inflamed tissue and is found on pathogenic T cells) (Supplementary Figure 4). An enhanced T cell presence was seen in the HIP with significantly more CD4+ T cells (Figure 6f) and increased fold changes in naïve CD4 (CD62L+CD44-, 2-fold), effector (CD62L-CD44+,4-fol) and T resident memory (TRM) (based on expression of CD69, CD103, CXCR6 or the combination of all,3-4-fold) populations between co-pathology and tau (Supplementary Figure 5)and only changes in CD8 naïve T cells (Figure 6g,h). Similar changes are seen across brain regions such as the CTX (Figure 6k,l) and the ENT (Figure 6o,p) with the most robust fold increases seen in CD4 and CD8 TRM populations in the CTX (4-fold) and CD4 TRMs in the ENT (1.2-fold), likely due to the transition of these infiltrating T cells into these regions, experienced antigen and maintaining CNS residence. In the MB and STR, T cell numbers in the co-pathology model compared to PFF were decreased (Figure 7c,g), with 1.5-fold increase in CD4+ Treg (CD25+) and CD8+ naïve populations in the MB (1.2-fold) (Figure7d,e) and CD4+ naïve populations in the STR (1.4-fold) (Figure 7h) however no fold changes with any CD8+ populations (Figure 7i) (Supplementary Figure 6). Given that there is only α-syn pathology present in the MB

and STR of co-pathology brains, the differential response (fewer total T cells but increase in Treg and naïve populations),our findings suggest, this change in T cell phenotype compared to the temporal and cortical regions may be due to the regional pathology and localized immune populations.

Using the aforementioned pipeline for high dimensional immune cell characterization, spectral flow cytometry was performed on co-pathology brains (Figure 8a). Using Python analysis for clustering, we identified 6 for CD4+ T cell clusters (Figure 8b) and 5 clusters for CD8+ T cells (Figure 8e), respectively. To identify how the T cells respond and are functioning in response to co-pathology across interconnected brain regions, changes between clusters were identified using markers for effector, activated, TRM, exhausted and anti-inflammatory subsets. Within the 6 clusters identified for CD4+ T cells in the co-pathology brains, Cluster 0 (early TRM, CD69+CD103lo) and 2 (effector/early TRM, CD69+CD44+), were not changed across brain regions while Cluster 1, transitioning Tregs (CD62L+CD25+) were enriched in the MB and CTX, with decreases in abundance in the HIP and ENT (Figure 8d). Clusters 3 and 4, effector cells (CD44+CD69loCD25+) and TRM (CD69+CD103+PD-1lo), respectively, were significantly enriched in the STR and HIP, respectively (Figure 8d). Exhausted TRM and non-effector exhausted TRM, Clusters 5 and 6, were also not changed across regions in the co-pathology brain (Figure 8d, Clusters 5 and 6). Across the landscape of CD8 T cell response in the co-pathology model, there were no significant changes in cluster enrichment of the non-pathogenic early TRM to more exhausted pathogenic TRM. CD8+ TRMs, however, seem to transition from Cluster 1 -> 0 -> 2 -> 3, indicative of enhanced activation followed by exhaustion, with changes in CXCR6 and PD-1 expression (Figure 8f,g). These results identify how T cells may also be responding, like

microglia, in response to pathology abundance based on brain region. Lastly, CD8+ T cells are all enriched for some TRM phenotypes, which do not change depending on brain region or pathology load (Figure 8g). Together, these results highlight how CD4 and CD8 T cells may function differently in eliciting an immune response in the co-pathology brain. Distinct changes and transitions in TRMs also provide evidence for infiltrating T cells potentially remaining in the brain and adopting a memory, tissue-resident phenotype to prolong the immune response.

Figures

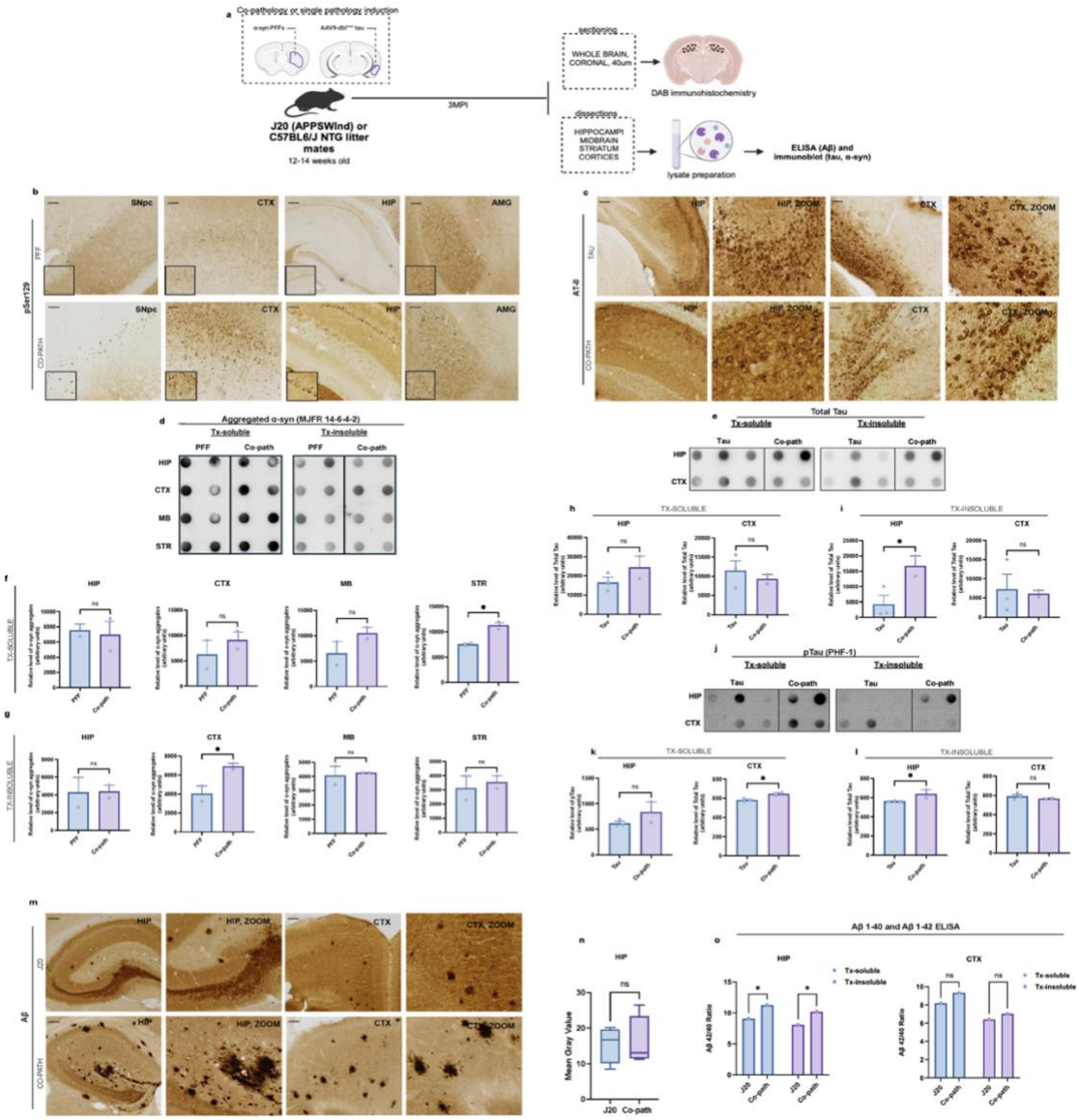

Figure 1. Co-pathology model induction results in seeding and accelerated pathology spread across the brain at 3MPI. (a) J20 transgenic and non-transgenic (NTG) littermates are injected at 12-14 weeks of age with 2uL of 5ug α-syn PFFs and 2uL of 3.2E12 vg/mL AAV double mutant tau into the dorsal lateral striatum and entorhinal cortex, respectively. For single pathology controls, non-transgenic (NTG) littermates are injected at 12-14 weeks old with α-syn PFFs into the dorsal lateral striatum for PFF single control or AAV double mutant tau into the entorhinal cortex for Tau single control. Age-matched J20 mice are used Aβ single pathology control. At 3

months post-induction (3MPI) rains were harvested and either PFA fixed for 40µm coronal sectioning or lysate prepared for dot blot or ELISA. (b) IHC images for pSer129 (DAB+, brown), in the substantia nigra pars compacta (SNpc), amygdala (AMG), cortex (CTX) and hippocampus (HIP) in both PFF single pathology controls and co-pathology model mice. Brightfield images taken at 20X, scale bars = 200µm. (d) Dot blot with PFF and co-pathology HIP, CTX, MB (midbrain, including SNpc) and STR soluble and insoluble fractions probed with aggregated α-syn antibody. (f,g) Quantification of dot blot signal intensity from each brain region in single pathology and co-pathology samples. n=2 brain regions/group. Student's t test used to test for significance. Graphs within display the mean +/- SEM. *$p<0.05$, ns= not significant. (c) IHC for pTau AT-8 (DAB, brown in the HIP and CTX of AAV-dbl^{mut} Tau single pathology controls and co-pathology model mice. Brightfield images taken at 20X. Scale bars = 200µm. (e,j) Dot blot with Tau and co-pathology HIP and CTX Triton X-100 soluble and insoluble fractions probed with total tau and PHF-1, respectively. (h,k,l) Resulting quantification compares the arbitrary units based on total tau or pTau intensity between groups. n=3 brain regions for tau group and n=2 brain regions for co-pathology group. Student's t test used to test for significance. Graphs within display the mean +/- SEM. *$p<0.05$. ns = not significant. (m) Aβ-positive extracellular plaques (DAB+ IHC, brown) are present in the HIP and CTX of J20 single pathology brains and co-pathology model brains. Brightfield images taken at 20X, scale bars = 200µm. (n) Mean gray value analysis compares Aβ load between these groups in the HIP. n=4/group. Student's t test used to test for significance. Graphs within display the mean +/- SEM. ns = not significant. (o) Aβ 42/40 ratio between J20 and co-pathology model mice on soluble and insoluble fractions. n=2-3/group were used. Two-way ANOVA used to test for significance. Graphs within display the mean. *$p<0.05$. Scale bars = 200µm.

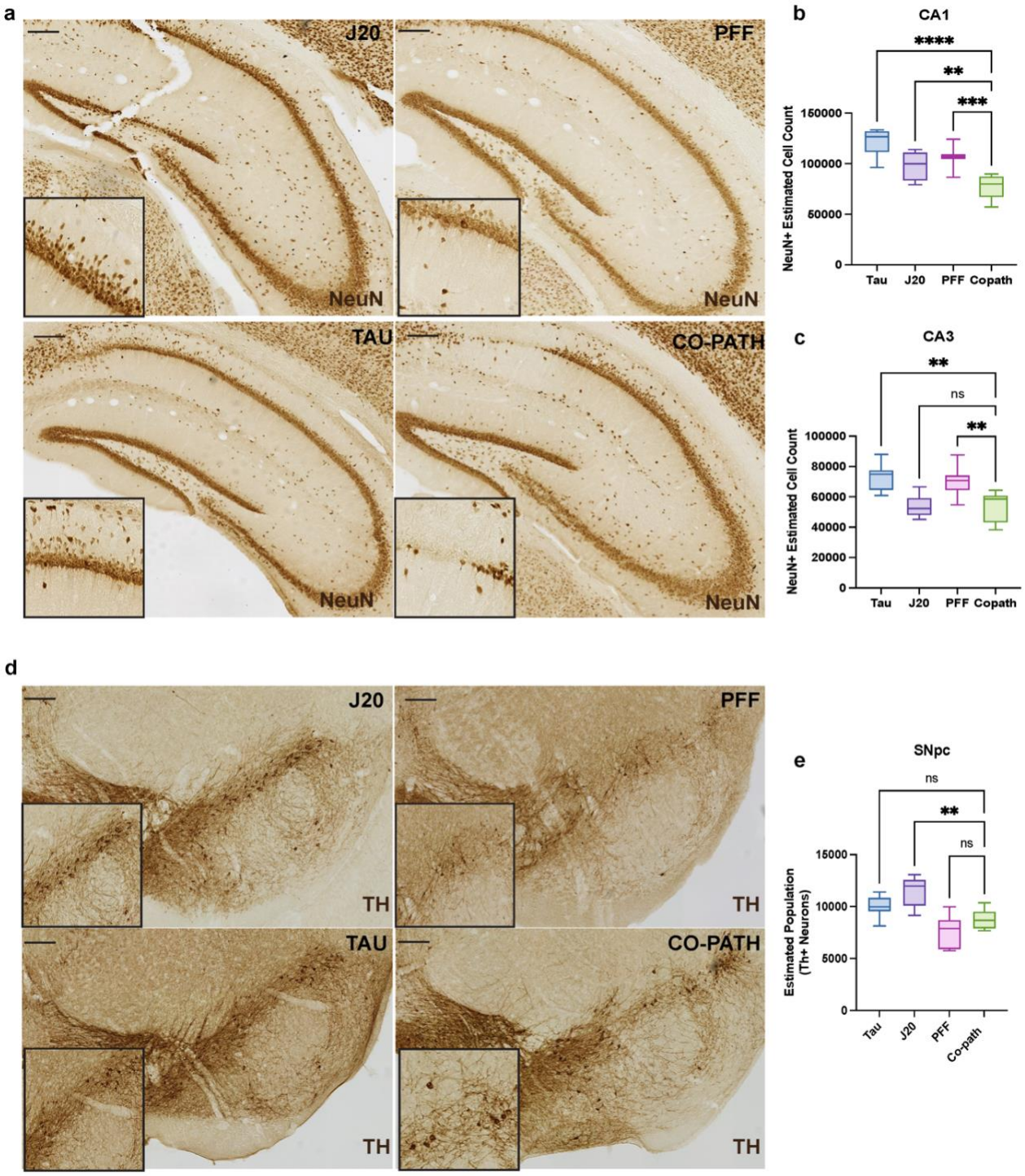

Figure 2. Brain-region specific neuronal loss is enhanced by the co-expression of α-syn, tau and Aβ. 6 MPI, animals were sacrificed and brains processed for IHC and unbiased stereology (a) Representative brightfield images of NeuN+ neurons (DAB+, brown) in the hippocampus. Images

taken at 20X. Scale bars = 300µm. (b,c) Unbiased stereology was used to quantify the number of NeuN+ neurons in the CA1 and CA3 regions of the hippocampus in the co-pathology mouse model compared to tau, PFF and J20 single pathology brains. n=8/group, both males and females. One-way ANOVA with post hoc for significance. Mean values +/- SEM are plotted. ns = no significance, **** $p<0.0001$, ***$p>0.005$, **$p<0.01$. n=7-8 animals per group. (d) TH+ neurons (DAB+, brown) were immunolabeled and representative brightfield images shown between Tau, PFF and J20 single pathologies and co-pathology mice. Brightfield images taken at 20X. Scale bars = 300µm. (e) Unbiased stereological cell counts for TH+ neurons in the SNpc compared between single pathology animals and co-pathology. One-way ANOVA with post hoc for significance. Mean values +/- SEM are plotted. ns = no significance, ****$p<0.0001$, ***$p>0.005$, **$p<0.01$. n=7-8 animals per group

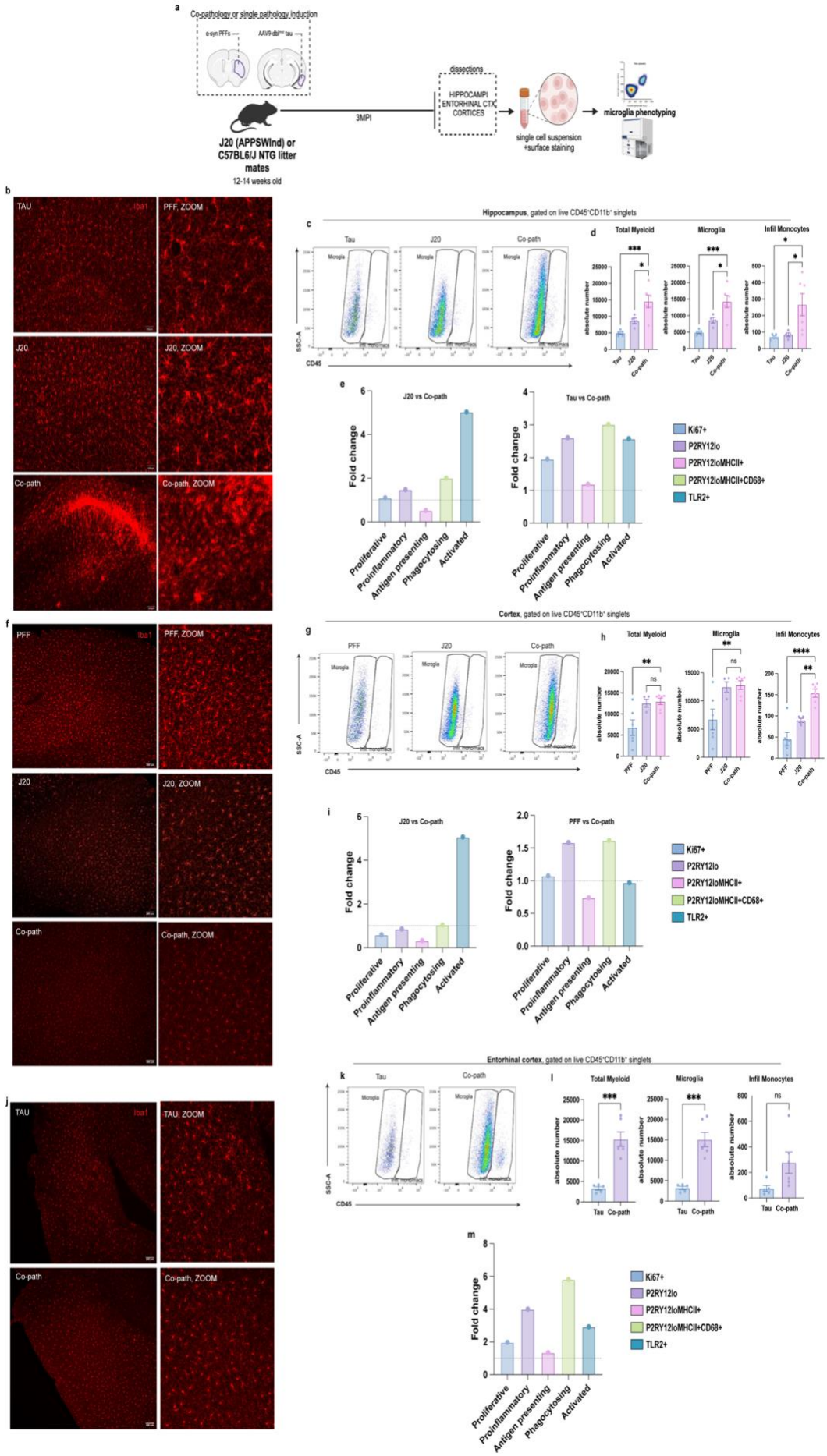
a
Co-pathology or single pathology induction
α-syn PFFs
AAV9-db/mt tau
J20 (APPSWInd) or C57BL6/J NTG litter mates
12-14 weeks old
3MPI
dissections
HIPPOCAMPI
ENTORHINAL CTX
CORTICES
single cell suspension +surface staining
microglia phenotyping
b
TAU
Iba1
PFF, ZOOM
J20
J20, ZOOM
Co-path
Co-path, ZOOM
c
Hippocampus, gated on live CD45+CD11b+ singlets
Tau
J20
Co-path
Microglia
SSC-A
CD45
d
Total Myeloid
Microglia
Infil Monocytes
absolute number
e
J20 vs Co-path
Tau vs Co-path
Fold change
Proliferative
Proinflammatory
Antigen presenting
Phagocytosing
Activated
Ki67+
P2RY12lo
P2RY12loMHCII+
P2RY12loMHCII+CD68+
TLR2+
f
PFF
PFF, ZOOM
J20
J20, ZOOM
Co-path
Co-path, ZOOM
g
Cortex, gated on live CD45+CD11b+ singlets
PFF
J20
Co-path
h
Total Myeloid
Microglia
Infil Monocytes
i
J20 vs Co-path
PFF vs Co-path
j
TAU
TAU, ZOOM
Co-path
Co-path, ZOOM
k
Entorhinal cortex, gated on live CD45+CD11b+ singlets
Tau
Co-path
l
Total Myeloid
Microglia
Infil Monocytes
m

Figure 3. Myeloid cells, including microglia and infiltrating monocytes are increased and activated under co-pathology conditions compared to single pathologies in the temporal and neocortical regions. (a) J20 transgenic and non-transgenic (NTG) littermates are injected at 12-14 weeks of age with 2uL of 5ug α-syn PFFs and 2uL of 3.2E12 vg/mL AAV double mutant tau into the dorsal lateral striatum and entorhinal cortex, respectively. For single pathology controls, non-transgenic (NTG) littermates are injected at 12-14 weeks of age with α-syn PFFs into the dorsal lateral striatum for PFF single control or AAV double mutant tau into the entorhinal cortex for Tau single control. Age-matched J20 mice are used Aβ single pathology control. n = 5-6/group, with two mouse brain regions pooled per sample, both males and females used. At 3MPI, brains were collected and the hippocampi, surrounding cortices and entorhinal cortices dissected, and single cells isolated and processed for flow cytometry. (b) Representative confocal images of Iba1 positive staining (red) in the hippocampus of tau, J20 and co-pathology mice to compare ramified (resting, homeostatic) vs more ameboid (activated) morphology between groups. Images taken at 10X. Scale bars = 100μm. (c) Representative flow cytometry dot blots of microglia (CD45 mid-lo) and infiltrating monocytes and macrophages (CD45hi) between co-pathology and single pathology conditions. (d) Flow plots are quantified showing the absolute total number of myeloid cells (CD45+CD11b+), which include microglia (CD45mid-lo) and infiltrating monocyte (CD45hi, Ly6C+) populations. (e) Fold change of microglial populations in co-pathology brains relative to single pathology brains show changes in proliferative (Ki67+), pro-inflammatory (P2RY12lo), activated (TLR2+), activated and antigen presenting (MHCII+) and phagocytosing (CD68+) microglia. Similar plots and results are shown for the (f-i) cortex and (j-m) entorhinal cortex. One-way ANOVA (for HIP and CTX) or student's t test (for ENT). Mean values +/- SEM are plotted. *$p<0.05$, **$p<0.01$, ***$p<0.005$.

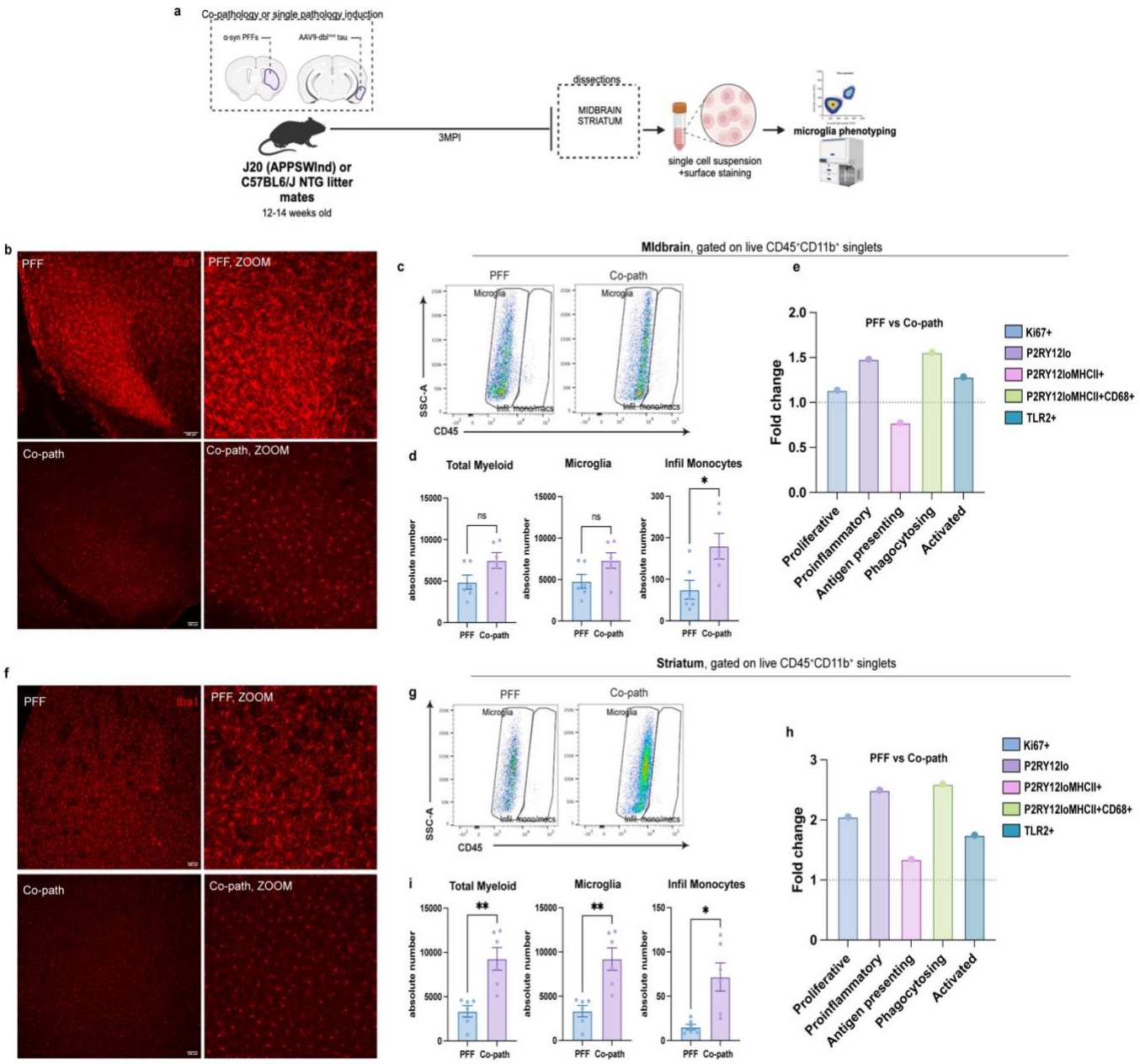

Figure 4. In the basal ganglia, microglia and infiltrating monocytes are increased and activated under co-pathology conditions compared to single pathologies. (a) J20 transgenic and non-transgenic (NTG) littermates are injected at 12-14 weeks of age with 2uL of 5ug α-syn PFFs and 2uL of 3.2E12 vg/mL AAV dbl^{mut} tau into the dorsal lateral striatum and entorhinal cortex, respectively. For single pathology controls, non-transgenic (NTG) littermates are injected

at 12-14 weeks of age with α-syn PFFs into the dorsal lateral striatum for PFF single control or AAV double mutant tau into the entorhinal cortex for Tau single control. Age-matched J20 mice are used Aβ single pathology control. n = 5-6/group, with two mouse brain regions pooled per sample, both males and females used in analysis. 3MPI, brains were collected and the HIP, CTX and ENT, and single cells isolated and processed for flow cytometry. (b) Representative images of Iba1 positive staining (red) in the SNpc of PFF and co-pathology mice to compare ramified (resting, homeostatic) vs more ameboid (activated) morphology between groups. Confocal images taken at 10X. Scale bars = 100μm. (c) Representative flow cytometry dot blots of microglia (CD45 mid-lo) and infiltrating monocytes and macrophages (CD45hi) between co-pathology and single pathology conditions in the midbrain. (d) Flow plots are quantified showing the absolute total number of myeloid cells (CD45+CD11b+), which include microglia (CD45mid-lo) and infiltrating monocyte (CD45hi, Ly6C+) populations. (e) Fold change of microglial populations in co-pathology brains relative to single pathology brains show changes in proliferative (Ki67+), pro-inflammatory (P2RY12lo), activated (TLR2+), activated and antigen presenting (MHCII+) and phagocytosing (CD68+) microglia. Similar plots and results are shown for the (f-i) STR. n = 5-6/group, with two mouse brain regions pooled per sample, both males and females used in analysis. Student's t-test used to test for significance. Mean values +/- SEM are plotted. *$p<0.05$, **$p<0.01$.

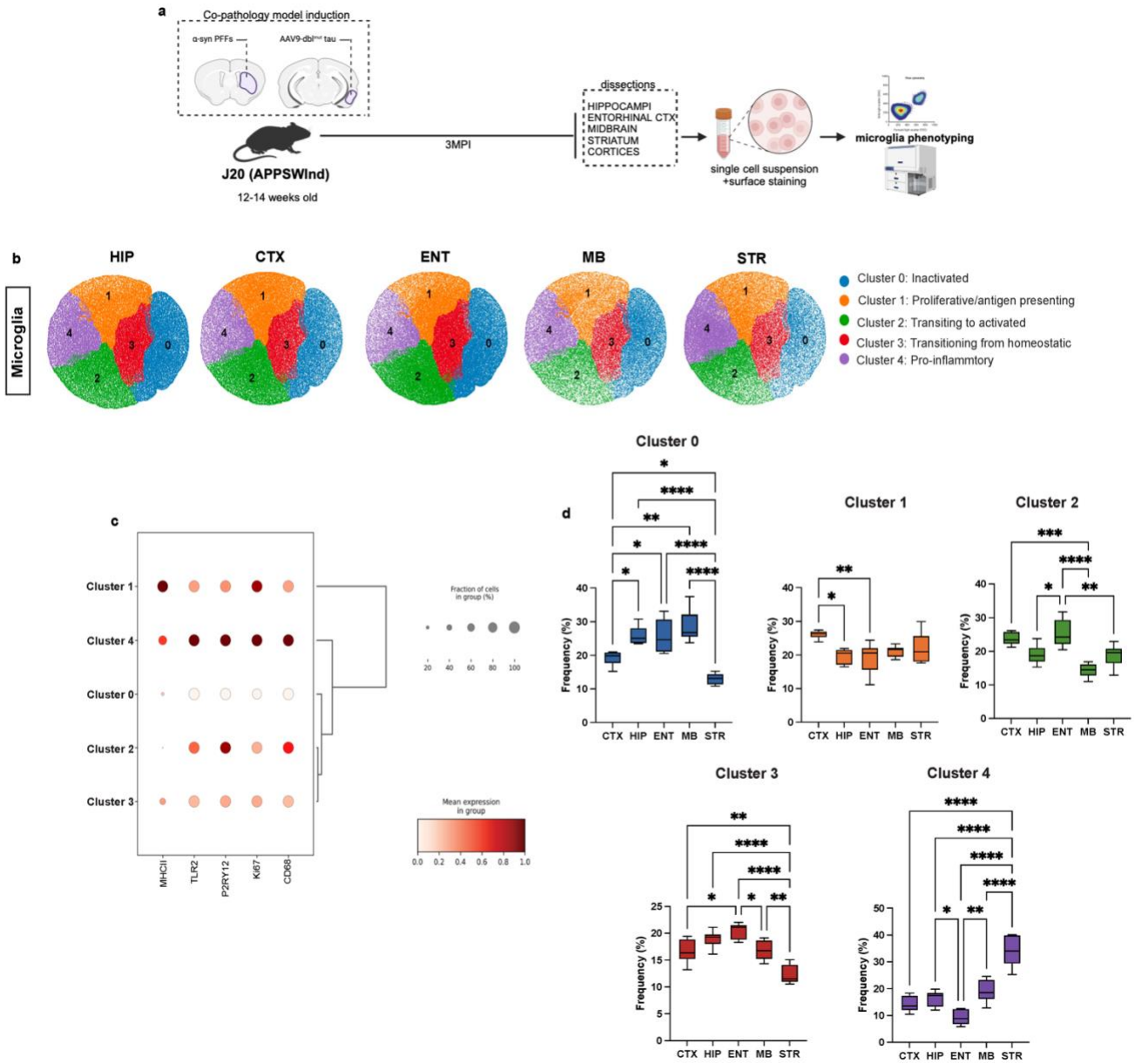

Figure 5. Activation state of microglia depends on abundance of protein pathology in the co-pathology brains. At 12-14 weeks of age, J20 mice were injected with α-syn mouse pre-formed fibrils (mPFFs) and AAV dbl^{mut} tau virus into the STR and ENT. At 3MPI, brains were collected and the HIP, CTX, STR, MB and ENT dissected for flow cytometry. n = 5-6/group, with two mouse brain regions pooled per sample, both males and females used. (b) UMAP plot showing the distribution of microglia categorized into 5 leiden clusters based on the expression profiles of 5

immunological markers: MHCII, TLR2, P2RY12, Ki67 and CD68. Cell numbers for each group are as follows: CTX = 76872 cells, ENT = 90424 cells, HIP = 85547 cells, MB = 43750 cells and STR = 55215 cells. (c) Clustering analysis reveals cellular subpopulations based on the protein marker expression for Cluster 0: inactivated (MHCIIlo), Cluster 1: proliferative/antigen presenting (MHCII+Ki67+TLR2midP2RY12midCD68mid), Cluster 2: transitioning to activated (P2RY12hiTLR2+CD68+Ki67mid), Cluster 3: transitioning from homeostatic (P2RY12mid) and Cluster 4: pro-inflammatory (TLR2+CD68+Ki67+CD68+). (d) Based on leiden frequency of cells within each cluster, percentage based on specific brain region are shown across the 4 clusters. One-way ANOVA used to test for significance. n = 5-6/group, with two mouse brain regions pooled per sample, both males and females used in analysis *$p<0.05$, **$p<0.0085$, ****$p<0.0001$.

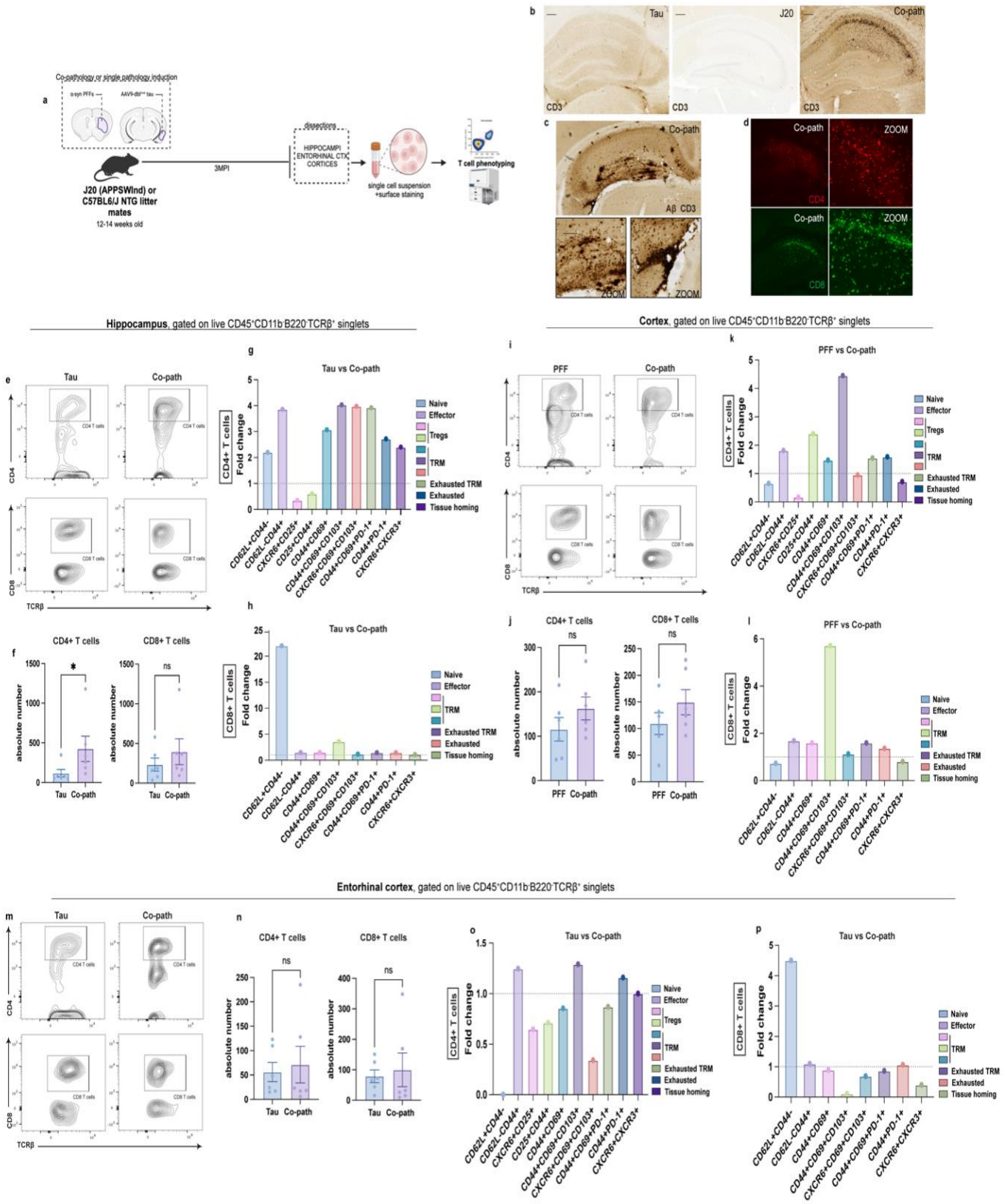

a
Co-pathology or single pathology induction
α-syn PFFs
AAV9-dbl™ tau
J20 (APPSWInd) or C57BL6/J NTG litter mates
12-14 weeks old
3MPI
dissections
HIPPOCAMPI ENTORHINAL CTX CORTICES
single cell suspension +surface staining
T cell phenotyping
b
Tau
J20
Co-path
CD3
c
Co-path
Aβ CD3
ZOOM
d
Co-path
ZOOM
CD4
CD8
Hippocampus, gated on live CD45+CD11b-B220-TCRβ+ singlets
Cortex, gated on live CD45+CD11b-B220-TCRβ+ singlets
e
Tau
Co-path
CD4
CD8
TCRβ
g
Tau vs Co-path
CD4+ T cells
Fold change
Naive
Effector
Tregs
TRM
Exhausted TRM
Exhausted
Tissue homing
CD62L+CD44-
CD62L-CD44+
CXCR6+CD25+
CD25+CD44+
CD44+CD69+
CD44+CD69+CD103+
CXCR6+CD69+CD103+
CD44+CD69+PD-1+
CD44+PD-1+
CXCR6+CXCR3+
i
PFF
Co-path
CD4
CD8
TCRβ
k
PFF vs Co-path
CD4+ T cells
Fold change
f
CD4+ T cells
CD8+ T cells
absolute number
*
ns
Tau
Co-path
h
Tau vs Co-path
CD8+ T cells
Fold change
j
CD4+ T cells
CD8+ T cells
ns
absolute number
PFF
Co-path
l
PFF vs Co-path
CD8+ T cells
Fold change
Entorhinal cortex, gated on live CD45+CD11b-B220-TCRβ+ singlets
m
Tau
Co-path
CD4
CD8
TCRβ
n
CD4+ T cells
CD8+ T cells
ns
absolute number
Tau
Co-path
o
Tau vs Co-path
CD4+ T cells
Fold change
p
Tau vs Co-path
CD8+ T cells
Fold change

Figure 6. Effector and exhausted CD4+ and CD8+ T cells are enriched in the co-pathology brain compared to single pathology controls in the temporal and neocortical regions. (a) J20 transgenic and non-transgenic (NTG) littermates are injected at 12-14 weeks of age with 2uL of 5ug α-syn PFFs and 2uL of 3.2E12 vg/mL AAV dbl^{mut} tau into the dorsal lateral striatum and entorhinal cortex, respectively. For single pathology controls, non-transgenic (NTG) littermates are injected at 12-14 weeks of age with α-syn PFFs into the dorsal lateral striatum for PFF single control or AAV double mutant tau into the entorhinal cortex for Tau single control. Age-matched J20 mice are used Aβ single pathology control. At 3MPI, brains were collected and the hippocampi, surrounding cortices and entorhinal cortices dissected and processed for spectral flow cytometry. n = 6/group, with two mouse brain regions pooled per sample, both males and females included in analysis. (b) Representative images of CD3+ T cells (DAB+, nickel) in the HIP between J20 and Tau single pathology controls and co-pathology mice. (c) Brightfield IHC images show double labeling of CD3 (nickel, black) and Aβ plaques (brown) in the hippocampus of co-pathology model mice. Bottom panel shows zooms of CD3 T cells surrounding plaques and entering though vessels in this region. Scale bars = 200μm. d) Representative confocal IHC images of the HIP of co-pathology model mice with CD4 (red) and CD8 (green). All images (both fluorescent and DAB), taken at 10X with digitally zoomed images. Scale bars = 200μm. (e) Flow cytometry dot plots of TCRβ+CD4+ (top panel) and TCRβ+CD8+ (bottom panel) T cells in the HIP of Tau and co-pathology mice. (f) Quantification of flow plots shows absolute cell number within each group of CD4+ and CD8+ T cells. Mean values +/- SEM are plotted and non-parametric Mann-Whitney test used to analyze for significance. ns = no significance. *$p<0.05$, **$p<0.01$. (g, h) Representative graph of the fold changes of populations of naïve (CD62L+), effector(CD44+), T-regulatory (Treg) cells(CD44+CD25+), tissue resident memory (TRM) cells

(expression of all or either CD69, CD103 or CXCR6), exhausted (PD-1+) and tissue homing/pathogenic (CXCR6+) CD4 and CD8 T cells in the co-pathology model relative to tau single pathology controls. Similar plots are shown for other collected brain regions including the (i) CTX and (m) ENT.

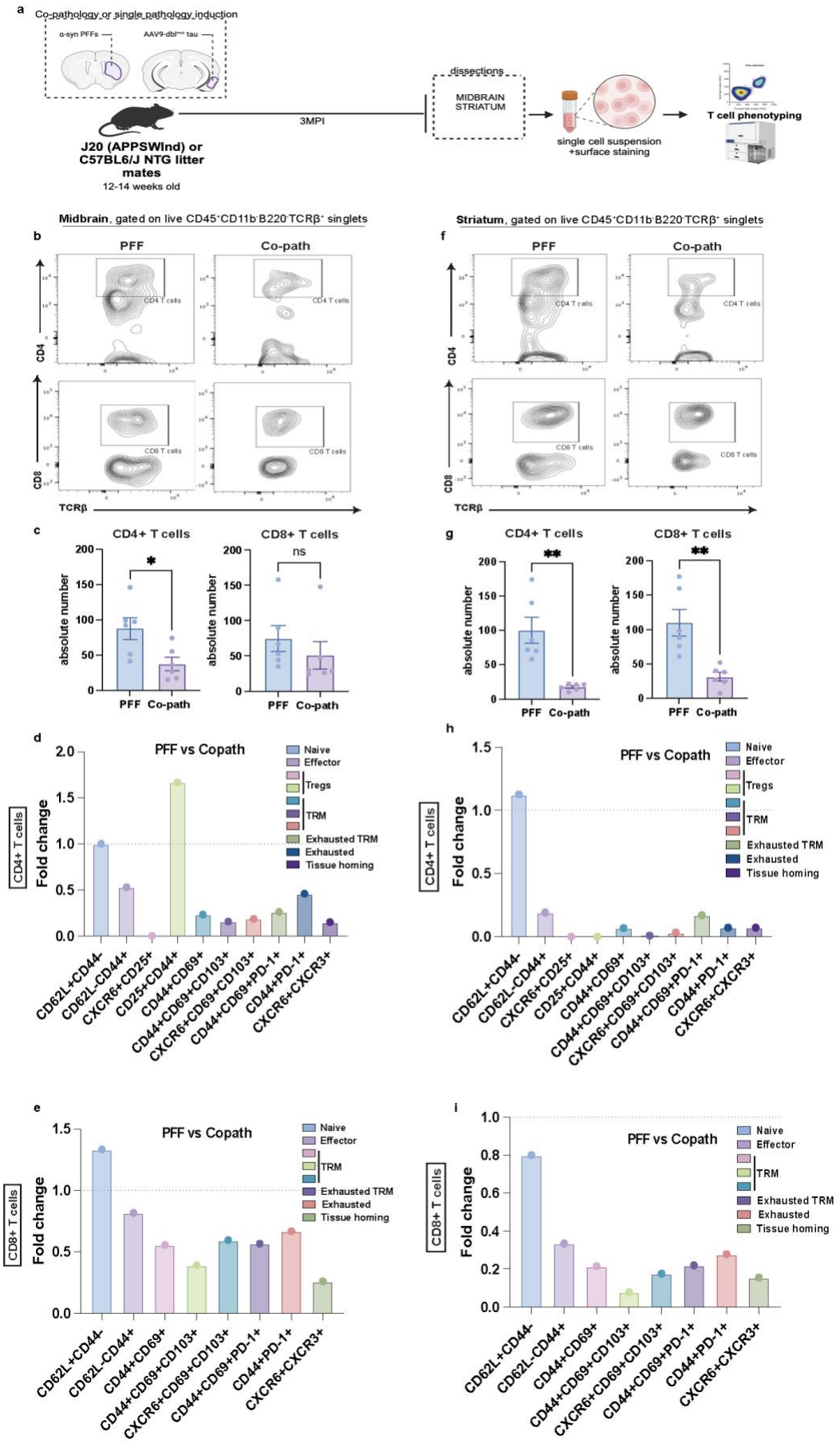
a
Co-pathology or single pathology induction
α-syn PFFs
AAV9-dbl^mut tau
J20 (APPSWInd) or C57BL6/J NTG litter mates
12-14 weeks old
3MPI
dissections
MIDBRAIN
STRIATUM
single cell suspension +surface staining
T cell phenotyping
Midbrain, gated on live CD45+CD11b-B220-TCRβ+ singlets
Striatum, gated on live CD45+CD11b-B220-TCRβ+ singlets
b
f
PFF
Co-path
CD4 T cells
CD8 T cells
CD4
CD8
TCRβ
c
g
CD4+ T cells
CD8+ T cells
absolute number
PFF
Co-path
ns
d
e
h
i
PFF vs Copath
CD4+ T cells
CD8+ T cells
Fold change
Naive
Effector
Tregs
TRM
Exhausted TRM
Exhausted
Tissue homing
CD62L+CD44-
CD62L-CD44+
CXCR6+CD25+
CD25+CD44+
CD44+CD69+
CD44+CD69+CD103+
CXCR6+CD69+CD103+
CD44+CD69+PD-1+
CD44+PD-1+
CXCR6+CXCR3+

Figure 7. Naïve and Treg CD4+ and Naïve CD8+ T cells are enriched in the basal ganglia of co-pathology brain compared to single pathology controls. a) J20 transgenic and non-transgenic (NTG) littermates are injected at 12-14 weeks of age with 2uL of 5ug α-syn PFFs and 2uL of 3.2E12 vg/mL AAV dbl^{mut} tau into the dorsal lateral STR and ENT. For single pathology controls, non-transgenic (NTG) littermates are injected at 12-14 weeks of age with α-syn PFFs into the dorsal lateral striatum for PFF single control or AAV double mutant tau into the entorhinal cortex for Tau single control. Age-matched J20 mice are used Aβ single pathology control. At 3MPI, brains were collected and the midbrain and striatum dissected and processed for flow cytometry. n = 6/group, with two mouse brain regions pooled per sample, both males and females used. (b) Resulting from spectral flow cytometry analysis, representative flow cytometry dot plots of TCRβ+CD4+ (top panel) and TCRβ+CD8+ (bottom panel) T cells in the midbrain of PFF and co-pathology mice. (c) Quantification of flow plots shows absolute cell number within each group of CD4+ and CD8+ T cells. Mean values +/- SEM are plotted and non-parametric Mann-Whitney test used to analyze for significance. ns = no significance. *$p<0.05$, **$p<0.01$. (g, h) Representative graph of the fold changes of populations of naïve (CD62L+), effector(CD44+), T-regulatory (Treg) cells(CD44+CD25+), tissue resident memory (TRM) cells (expression of all or either CD69, CD103 or CXCR6), exhausted (PD-1+) and tissue homing/pathogenic (CXCR6+) CD4 and CD8 T cells in the co-pathology model relative to PFF single pathology controls. Similar plots are shown for the striatum (f-l).

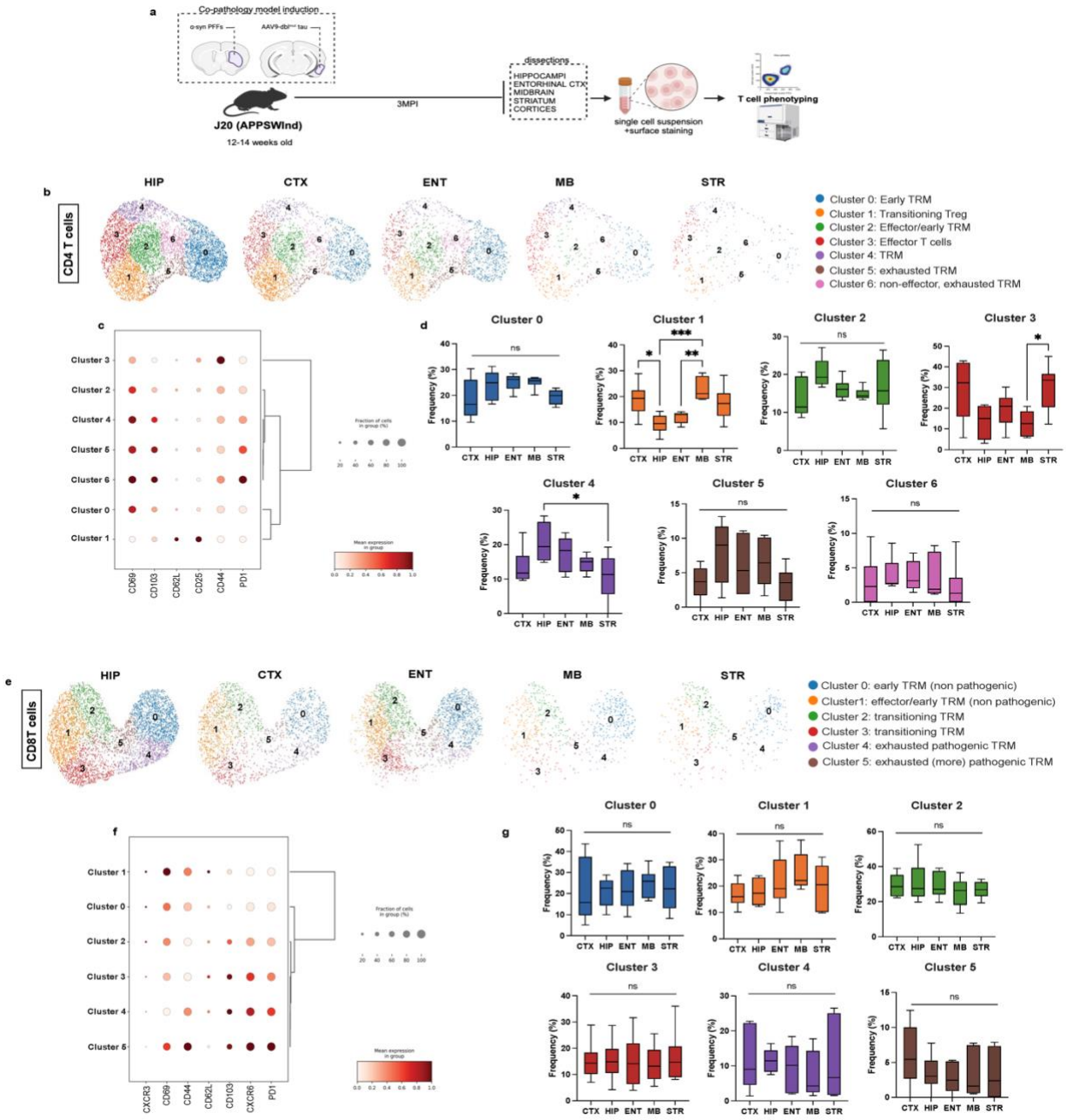

Figure 8. T cells differ in expression and activation state depending on abundance of protein co-pathology. a) At 12-14 weeks of age, J20 mice were injected with α-syn mouse pre-formed fibrils (mPFFs) and AAV dbl^{mut} tau virus into the striatum and entorhinal cortex, respectively, to induce the co-pathology model. At 3MPI, brains were collected and the HIP, CTX, STR, MB and ENT dissected for spectral flow cytometry. n = 6/group, with two mouse brain regions pooled per

sample, both males and females used. (b) UMAP plot showing the distribution of CD4 T cells categorized into 7 leiden clusters based on expression profiles of 6 immunological markers: CD69, CD103, CD62L, CD25, CD44 and PD1. Each cluster is uniquely numbered and color-coded. Cell numbers for each group are as follows: CTX = 3370 cells, ENT = 2179 cells, HIP = 7096 cells, MB = 781 cells and STR = 364 cells. (c) Clustering analysis reveals cellular subpopulations based on the protein marker expression for Cluster 0: early tissue resident memory (TRM) (CD69+CD103lo), Cluster 1: transitioning Treg (CD62L+CD25+), Cluster 2: effector early TRM (CD69+CD44+), Cluster 3: Effector (CD44+CD25+CD69loPD-1lo), Cluster 4: TRM (CD69+CD103+PD-1+), Cluster 5: exhausted TRM (CD69+CD103+PD-1+) and Cluster 6: non-effector, exhausted TRM (CD69+CD103+PD-1+CD44lo). (d) Based on leiden frequency of cells within each cluster, percentage based on specific brain region are shown across the 6 clusters. (e) UMAP plot showing the distribution of CD8 T cells categorized into 6 leiden clusters based on expression profiles of 6 immunological markers: CXCR3, CD69, CD44, CD62L, CD103, CXCR6 and PD1. Each cluster is uniquely numbered and color-coded. Cell numbers for each group are as follows: CTX = 2098 cells, ENT = 2579 cells, HIP = 5538 cells, MB = 749 cells and STR = 451 cells. (f) Clustering analysis reveals cellular subpopulations based on the protein marker expression for Cluster 0: early TRM (non-pathogenic) (CD69+CD44lo), Cluster 1: (non pathogenic) effector/early TRM (CD69hiCD44+), Cluster 2: transitioning TRM (CD69+CD103+CXCR6lo), Cluster 3: transitioning pathogenic TRM (CD103+CXCR6+PD-1lo), Cluster 4: exhausted TRM (CD44loCD103+CXCR6+PD-1+) and Cluster 5: exhausted pathogenic TRM (CD69+CD44+CD103+CXCR6+PD-1+). (g) Based on leiden frequency of cells within each cluster, percentage based on specific brain region are shown across the 6 clusters. One-way

ANOVA used to test for significance. Mean values +/- SEM are plotted *p<0.05, **p<0.0085, ****p<0.0001.

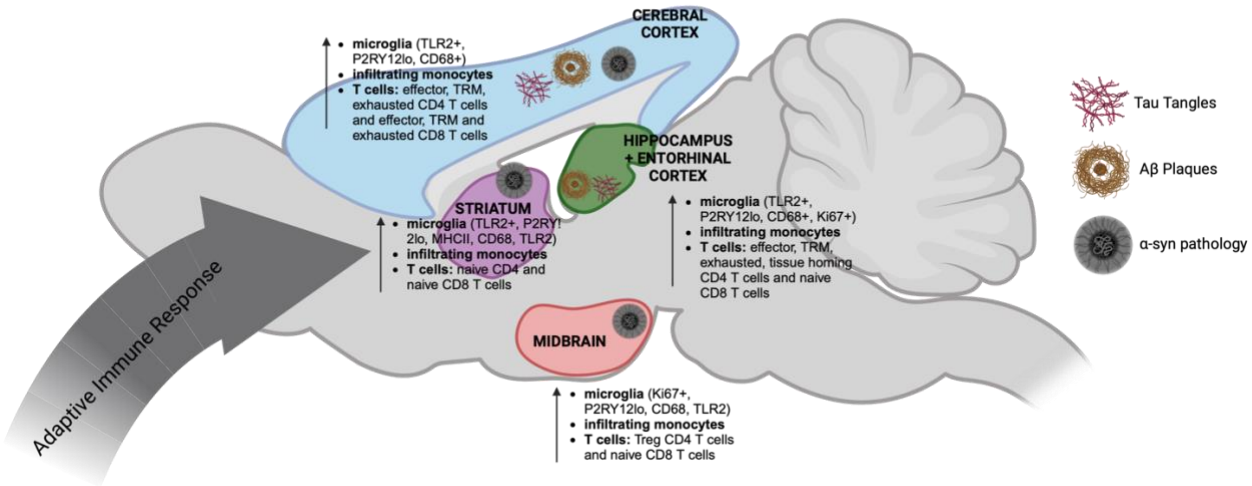

Figure 9. Differential innate and adaptive immune responses are elicited by the induction of co-pathologies and the subsequent spread and seeding of α-syn, tau and Aβ. The presence of α-syn, tau and Aβ co-pathologies within the cortices, hippocampus, striatum and midbrain, elicit changes in the innate and adaptive immune response. Changes in each brain region are summarized as follows: In the cortex (blue), there is an increase in infiltrating monocytes (Ly6C+) and microglia increase in number with an activated phenotype (TLR2, CD68 and low P2RY12 expression). CD4 T cells in this region show an effector and TRM phenotype with exhausted CD8 T cells. In the hippocampus and entorhinal cortex (green), Ly6Chi infiltrating monocytes are also present, with an increase in the number of activated, proliferating microglia as well as increase in the number T cells, specifically in CD4 T cells positive for markers of TRM, tissue homing and effector phenotypes. CD8 T cells in this brain region were mainly naïve. In the midbrain (pink), there was not a significant increase in the number of microglia, however, there were increased

proliferating and activation markers. With infiltrating monocytes there was not an increase in infiltrating T cells, but changes in CD4 Treg expression and naïve CD8 T cells, when compared to single pathologies. Lastly, in the striatum (purple), microglia and infiltrating monocytes were abundant with mainly activated, phagocytosing and proliferative microglia. T cells were decreased overall but were enriched for a naïve phenotype for both CD4 and CD8.

Discussion

α-syn, tau and Aβ as co-pathologies highlight an important factor in neurodegenerative disease, however how these protein pathologies synergize to enhance neurodegeneration is unknown. In studies within, we demonstrate using a novel mouse model of co-pathology incorporating α-syn, tau, and Aβ co-pathologies that the enhanced neuropathology and neurodegeneration may be due in part to the robust innate and adaptive immune response driven by the co-expression of these accumulated proteins At 3MPI, abnormal protein pathology load was enhanced compared to the single pathology controls along with a robust neuroinflammatory response, including increased microglial cell number, changes in activation markers, CD68 and TLR2, and MHCII expression, a complex important for antigen presentation. This effect of co-pathologies on abnormal protein pathology, neuroinflammation, and neurodegeneration were compared to the individual pathology controls, supporting the hypothesis that these protein pathologies collectively may drive the progression of disease.

To establish a co-pathology mouse model of neurodegenerative disease, we selected the J20 mouse line due to its moderate, localized Aβ plaque load in the hippocampus and cortex (Figure 1e, 2b) beginning at around 3-4 months of age as a result of the overexpression of human

mutant amyloid protein precursor (Swedish (K670N/M671L) and Indiana mutations (V717F)) [44]. These mice show selective hippocampal neuronal loss in the CA1 region after 12 weeks of age and increase in CD68+ activated microglia in the hippocampus [45]. Deficits in synaptic transmission and loss of synapses between neurons within the CA1 compared to non-transgenic mice have also been reported [46]. In recent studies, Aβ transgenic mice, 5xFAD and 3xTg [47], have been used to model co-pathologies including α-syn and tau. In one study 3xTg mice, that develop both Aβ plaques and tau neurofibrillary tangles, were crossed with M83 transgenic mice to create the first triple pathogenic model in the context of AD and DLB/AD [26]. Similarly, 5xFAD mice, that only develop Aβ pathology, were stereotaxically injected with mouse α-syn PFFs to develop a 'PDAD' [27] mouse. Crossing APP/PS1 mice with mutant P301L tau mice has also shown increased formation of Aβ plaques and tau tangles[48]. The mechanism underlying this has been linked to Aβ plaques activating kinases, which leads to mislocalization of tau, and subsequent hyperphosphorylation [48, 49]. Between tau and α-syn, 'cross-seeding' effects have been shown where tau can promote the formation of α-syn fibrils and vice versa[50]. Despite the discoveries made within these models and the validation of the synergistic properties of these pathologies when in the same environment, J20 mice more accurately model amyloid burden based on the localized expression in the hippocampus and cortex and synaptic degermation seen in age-related neurodegenerative diseases. To model pTau pathology in mice, we selected an adeno-associated virus AAV dbl^{mut} tau to overexpress tau in neurons within the entorhinal cortex. As endogenous mouse tau does not aggregate or form neurofibrillary tangle-like inclusions [51-53], it is a priority to induce the pathology in a region, like the entorhinal cortex, where localization and tracking allows for the propagation and subsequent expression of intracellular p-tau within the hippocampus and neighboring cortices. To simplify breeding and eliminate any potential issues

with crossing, we opted to combine the existing transgenic model with AAV dbl^{mut} tau. Lastly, to model Lewy-like pathology in the mouse brain, we selected a single 5ug injection of α-syn PFFs to induce intracellular Lewy-neurite and Lewy-body-like inclusions throughout the limbic system. Pathology was also observed intracellularly within the amygdala, cortex, hippocampus and other basal ganglia regions such as the striatum and the midbrain, specifically the substantia nigra pars compacta. While AAVs that overexpress α-syn in transduced regions have been used to model PD[54-57], these overexpression vectors typically lack the disease-like spreading pathology and only recapitulate the molecular pathology of SNCA duplication/triplication carriers [58, 59]. Although this co-pathology mouse model does not fully reflect the spatial representation of these pathologies, with Aβ and tau found in other regions, our goal was to induce pathology within regions of origination in their classically designated diseases. Despite these factors, we found that with the combination of AAV dbl^{mut} tau and PFFs with the J20 line, we can consistently recapitulate the effect of these pathologies across varying brain regions. Future studies will need to focus on creating mouse model with improved spatial-temporal resolution with pathology in interconnect brain regions to more accurately depict human disease. This will be crucial in elucidating the role of the order of presence, timing, and location of these pathologies on disease progression.

Neuronal loss is a hallmark of neurodegenerative diseases and has been well documented in both postmortem brains and animal models. In PD, up to 80% of dopaminergic neurons are lost from the substantia nigra pars compacta, which correlates with the onset and severity of motor impairments [60]. During the early stages of AD, before the presence of neurofibrillary tangles, 25%-40% of neurons in the entorhinal cortex are lost [61, 62], with 50%-60% of neurons and synapses [63] in the hippocampus and neocortex being lost later on in disease, initiating the onset of cognitive decline. Here, we show that the presence of co-pathology results in enhanced neuronal

loss specifically in the CA1 and CA3 regions of the hippocampus compared to single pathology controls (Figure 2a,b), correlating with enhanced pathology load and elevated immune responses. Within the SNpc specifically, the presence of co-pathologies resulted in significant loss of TH+ neurons between J20 single pathology and co-pathology animals at 6MPI, and not the PFF and tau single pathology mice (Figure 2d). The lack of significant loss in the co-pathology SNpc compared to PFF and tau single pathology animals, contrary to what is seen in the hippocampus, is likely due to the localization and abundance of the co-expression of these proteins in these varying brain regions. In support, within the hippocampus, whether at 3MPI or 6MPI, we show the induction of all three pathologies while the SNpc only has significant α-syn inclusions. This leads us to consider the potential of modeling more AD or PD-dementia, and not a pure synucleinopathy due to localized neuronal loss in the hippocampus. In support, a recent study in postmortem PD and Parkinsonism indicated the initiation of SNpc dopaminergic neurodegeneration occurs independently of α-syn aggregation and may be initially mediated by tau [64]. Future studies are warranted to determine the causative or additive role Tau in addition to α-syn in dopaminergic neurodegeneration.

Longitudinal and post-mortem studies from PD and AD cohorts show earlier onset of cognitive decline and higher mortality rates with the presence of co-pathologies [65, 66]. Based on this, pure pathology is not common and may not be associated with the cognitive impairment onset in these neurodegenerative diseases [67-69]. In pre-clinical models, behavioral phenotypes are also important for confirming these results, and studies were performed to assess both motor and cognitive deficits. In the co-pathology mice no significant exacerbation of behavioral phenotypes was observed compared to individual controls (data not shown). This may be due in

part to the nature of the mice, his maybe in part due to the baseline hyperactivity of the J20 mice or a potential celling effect observed within the J20 mice independent of co-pathologies. Future studies with more specific tests may be more sensitive in detecting both cognitive and motor deficits without this confounding factor. In the α-syn PFF model, no significant motor deficits were detected compared to α-syn monomer control, likely due to the 30-50% TH+ neuron loss not meeting the critical threshold as observed in other studies[70]. Despite these challenges, we are still able to show what may be the beginning of a more robust neuronal loss in the hippocampus and SNpc, which does support a more accurate model of neurodegeneration.

Microglial activation and the infiltration of T cells is well documented in response to Aβ, tau and α-syn individually in AD and PD [71-75]. However, studies implicating the role of inflammation in driving neurodegeneration in a co-pathology pre-clinical model are lacking. In most co-pathology models there is a large gap in understanding is how the presence of co-pathologies activates immune responses. Utilizing the novel co-pathology model as well as individual pathology controls, we are able to show that the co-expression of these pathologies induces robust changes in microglia, and enhances infiltrating monocytes and T cells. Compared to single pathologies, the presence of co-pathologies resulted in increased number of total myeloid cells in the hippocampus, cortex, entorhinal cortex and the striatum (Figure 3,4). Most of these activated cells are CNS microglia. Infiltrating monocytes and other resident macrophages also make up a significant portion of this population, however it is less compared to microglia. Our findings are consistent with recent work in postmortem tissue that compared microglia reactivity between mixed pathology (DLB+AD) brains, showing higher loads of CD68, reactive microglia in the amygdala and hippocampus [69]. Spiked microglial load and activation state were strongly

associated with regions of Aβ, tau and to a lesser extent, α-syn. In addition to innate immune changes, we also demonstrate enhanced T cell responses compared to single pathologies, specifically in the hippocampus. In comparison to single pathology controls, both CD4+ and CD8+T cells showed changes in their inflammatory signatures, mostly shifting to tissue resident memory and effector phenotypes. In the midbrain, however, the overall number of T cells with co-pathology conditions were decreased, with increased naïve populations. This change in T cell number may be due to the lack of co-pathologies in this region. Interestingly, microglia numbers were not increased in this region. Microglia may respond differently in these regions based on the local environment, abundance of pathology, or the presence of other immune cells assisting with this pro-inflammatory response. This has been shown in other studies, where microglial gene expression varies between brain regions in response to both aging and neurodegeneration [76] and based on abundance and localization of Aβ plaques and tau pathology [77]. Changes in the T cell populations are likely due to pathology-driven antigens that are more abundant and more neurotoxic in the co-pathology conditions compared to that in single pathology brains. Based on the robust number of T cells in the hippocampus compared to other brain regions, this may also be a driving factor of the enhanced regional neurodegeneration and potential cognitive decline. With changes in pathology load, the pro-inflammatory environment created by the microglia and T cell interactions may also be promoting a lack of clearance of these proteins, and potentially increase expression. Single pathology, tau, PFF and J20, brains also showed higher populations of anti-inflammatory T-regulatory (Tregs) cells with co-pathologies having little to no expression of this population. This validates work seen in human PD patients, where Tregs are decreased, in the blood and brain, with disease progression [78-80], likely due to an overload of pathologies and a need for more pro-inflammatory cells and responses. The differences in T cell response may be

due to immune environment, influenced by α-syn, might differ compared to single pathology PFF controls. With PFFs, the immune response is focused on controlling α-syn pathology leading to infiltration of T cells. With co-pathologies, however, the overall co-pathology environment in the brain may result in a differential immune regulation in the MB and STR, leading to this increase in Treg populations that would play a role in limiting neuroinflammation and recruiting less effector T cells. Studies have also shown that Tregs can limit microglial activation[81], which has been shown within our model in the MB (Figure 4d).

Varying cell types and more importantly, brain regions have differential vulnerability to Aβ, tau and α-synuclein pathology. The effect of a co-pathology environment on this vulnerability has not been explored, especially in the context of linking pathology load and immune responses across brain regions. With both T cell and microglia changes based on pathology load in the temporal versus basal ganglia-related regions, we show region-specific immune responses, showing that areas with higher pathology load (more co-expression) have increased number of immune cells and more resident, pro-inflammatory phenotypes. The co-expression of pathologies amplifies microglial activation, likely through interactions with TLR2+ to activate NFκB signaling. TRM have been shown to exacerbate disease [15, 82] through pro-inflammatory cytokine release and cytolytic functions as well as by modulating the response by attracting and further activating microglia. The increase in TRM implies that these populations are not only recruited but are also retained due to local antigen presentation and chronic inflammation, likely from the microglia. Additionally, with the enrichment of Tregs alongside no increase in microglia in the MB, ours and other studies suggest that Tregs may be modulating microglial activation, which in turn reduces neuroinflammation and may subsequently protect neurons from death. This

may also explain our lack of TH+ neuronal loss in the SNpc compared to PFF and Tau single pathology controls.

Current therapeutic approaches target the removal of these protein pathologies, but primarily focus on the removal of individual pathologies. While controversial on whether it is disease modifying, Aducanumab has been utilized to target Aβ plaques to reduce the accumulation of these plaques in the brain. Recent studies in animal models have observed effects on the phagocytosing capabilities of microglia, which affects overall neuroinflammation and subsequent clearance of plaques. In PD, several studies have targeted α-syn, with promising results from approaches like monoclonal antibodies that aim to reduce the aggregation and spread of these inclusions [83, 84]. The singular targeting of pathologies and subsequent minimal changes in disease imply the need for multi-targeted interventions that may address the influence of the co-pathologies seen in neurodegenerative disease. Our model has shown a crucial association between regions of co-pathology, inflammation, and neuropathology. This highlights a need for combination therapy targeting multiple aggregated inclusions, or the inflammatory response within this co-pathology environment.

Altogether, our co-pathology model has shown that a CNS-driven immune response correlates with co-pathology expression (Figure 9), a common factor seen in human PD and AD patients, and that increased protein pathology load and neurodegeneration co-evolve with this environment. This model provides a powerful tool for investigating the role co-pathologies on neuroinflammation and neuropathology and provides a novel tool for combinational approaches for therapeutic targeting.

Declarations

Acknowledgements

We thank the UAB Comprehensive Flow Cytometry Core for their assistance with flow cytometry experiments. Experimental design figures were generated using BioRender. We would like to thank Josh Randolph for his consistent efforts and assistance with animal husbandry and handling. We thank Rajesh Gupta and Anna Stoll for their invaluable contributions to immunohistochemistry staining. We also thank Laura Volpicelli-Daly, Charlotte Brzozowski, Marissa Menard and Arielle Manabat for their invaluable contribution of PFFs and biochemical protocols and antibodies for our studies. Lastly, we would like to thank Warren Hirst, Lucas Hampton, Jeremy Herskowitz and Kelsey Greathouse for the assistance and advice for this project.

Competing interests

The authors have no competing interests.

Funding

This work was supported by a grant from the ASAP (Aligning Science Across Parkinson's) network (Grant# ASUB00000984).

Author's contributions

JMW and ASH designed the study and experiments and wrote the manuscript. JMW was responsible for stereotaxic surgeries. WJS conducted all ELISA and immunoblotting experiments and analysis. JMW, YTY, NJCS, GMC, ATM and AZ contributed towards tissue collection and

executing flow cytometry experiments. DTT provided code and assisted with the spectral flow python pipeline to analyze the T cell and microglia dataset. JMW conducted all IHC stains. NM conducted confocal microscopy for fluorescent images. JMW assessed NeuN+ stereology. AZ manually assessed Th+ stereology and JM developed AI pipeline to assess and confirm Th+ stereology. JMW and ASH drafted and constructed the manuscript and figures. FPM and IS developed and optimized the AAV double-mutant tau vector. FPM, JK and DJT provided feedback and edits to the manuscript. All authors read and approved the final manuscript.

References

1. Goedert, M., *Tau protein and the neurofibrillary pathology of Alzheimer's disease.* Trends Neurosci, 1993. **16**(11): p. 460-5.
2. Joachim, C.L. and D.J. Selkoe, *Amyloid protein in Alzheimer's disease.* J Gerontol, 1989. **44**(4): p. B77-82.
3. Spillantini, M.G., et al., *Alpha-synuclein in Lewy bodies.* Nature, 1997. **388**(6645): p. 839-40.
4. Irwin, D.J., et al., *Neuropathological and genetic correlates of survival and dementia onset in synucleinopathies: a retrospective analysis.* Lancet Neurol, 2017. **16**(1): p. 55-65.
5. Irwin, D.J., et al., *CSF tau and β-amyloid predict cerebral synucleinopathy in autopsied Lewy body disorders.* Neurology, 2018. **90**(12): p. e1038-e1046.
6. Jellinger, K.A., *Alzheimer disease and cerebrovascular pathology: an update.* J Neural Transm (Vienna), 2002. **109**(5-6): p. 813-36.
7. Jellinger, K.A., *Alpha-synuclein pathology in Parkinson's and Alzheimer's disease brain: incidence and topographic distribution--a pilot study.* Acta Neuropathol, 2003. **106**(3): p. 191-201.
8. Jellinger, K.A., *Neuropathological assessment of the Alzheimer spectrum.* J Neural Transm (Vienna), 2020. **127**(9): p. 1229-1256.
9. Kotzbauer, P.T., et al., *Pathologic accumulation of α-synuclein and Aβ in Parkinson disease patients with dementia.* Arch Neurol, 2012. **69**(10): p. 1326-31.
10. Robinson, J.L., et al., *Neurodegenerative disease concomitant proteinopathies are prevalent, age-related and APOE4-associated.* Brain, 2018. **141**(7): p. 2181-2193.
11. Spires-Jones, T.L., J. Attems, and D.R. Thal, *Interactions of pathological proteins in neurodegenerative diseases.* Acta Neuropathol, 2017. **134**(2): p. 187-205.
12. Compta, Y., et al., *The significance of α-synuclein, amyloid-β and tau pathologies in Parkinson's disease progression and related dementia.* Neurodegener Dis, 2014. **13**(2-3): p. 154-6.
13. Coughlin, D., et al., *Cognitive and Pathological Influences of Tau Pathology in Lewy Body Disorders.* Ann Neurol, 2019. **85**(2): p. 259-271.
14. Mak, E., et al., *Influences of amyloid-β and tau on white matter neurite alterations in dementia with Lewy bodies.* NPJ Parkinsons Dis, 2024. **10**(1): p. 76.
15. Gate, D., et al., *Clonally expanded CD8 T cells patrol the cerebrospinal fluid in Alzheimer's disease.* Nature, 2020. **577**(7790): p. 399-404.
16. Itagaki, S., P.L. McGeer, and H. Akiyama, *Presence of T-cytotoxic suppressor and leucocyte common antigen positive cells in Alzheimer's disease brain tissue.* Neurosci Lett, 1988. **91**(3): p. 259-64.
17. Merlini, M., et al., *Extravascular CD3+ T Cells in Brains of Alzheimer Disease Patients Correlate with Tau but Not with Amyloid Pathology: An Immunohistochemical Study.* Neurodegener Dis, 2018. **18**(1): p. 49-56.
18. Rogers, J., et al., *Expression of immune system-associated antigens by cells of the human central nervous system: relationship to the pathology of Alzheimer's disease.* Neurobiol Aging, 1988. **9**(4): p. 339-49.
19. Togo, T., et al., *Occurrence of T cells in the brain of Alzheimer's disease and other neurological diseases.* J Neuroimmunol, 2002. **124**(1-2): p. 83-92.

20. Brochard, V., et al., *Infiltration of CD4+ lymphocytes into the brain contributes to neurodegeneration in a mouse model of Parkinson disease.* J Clin Invest, 2009. **119**(1): p. 182-92.
21. Sulzer, D., et al., *T cells from patients with Parkinson's disease recognize α-synuclein peptides.* Nature, 2017. **546**(7660): p. 656-661.
22. Yan, Z., et al., *Dysregulation of the Adaptive Immune System in Patients With Early-Stage Parkinson Disease.* Neurol Neuroimmunol Neuroinflamm, 2021. **8**(5).
23. Hamza, T.H., et al., *Common genetic variation in the HLA region is associated with late-onset sporadic Parkinson's disease.* Nat Genet, 2010. **42**(9): p. 781-5.
24. Jimenez-Ferrer, I. and M. Swanberg, *Immunogenetics of Parkinson's Disease*, in *Parkinson's Disease: Pathogenesis and Clinical Aspects*, T.B. Stoker and J.C. Greenland, Editors. 2018, Codon Publications
Copyright: The Authors.: Brisbane (AU).
25. Harms, A.S., et al., *MHCII is required for α-synuclein-induced activation of microglia, CD4 T cell proliferation, and dopaminergic neurodegeneration.* J Neurosci, 2013. **33**(23): p. 9592-600.
26. Clinton, L.K., et al., *Synergistic Interactions between Abeta, tau, and alpha-synuclein: acceleration of neuropathology and cognitive decline.* J Neurosci, 2010. **30**(21): p. 7281-9.
27. Bassil, F., et al., *Amyloid-Beta (Aβ) Plaques Promote Seeding and Spreading of Alpha-Synuclein and Tau in a Mouse Model of Lewy Body Disorders with Aβ Pathology.* Neuron, 2020. **105**(2): p. 260-275.e6.
28. Bassil, F., et al., *α-Synuclein modulates tau spreading in mouse brains.* J Exp Med, 2021. **218**(1).
29. Luk, K.C., et al., *Exogenous alpha-synuclein fibrils seed the formation of Lewy body-like intracellular inclusions in cultured cells.* Proc Natl Acad Sci U S A, 2009. **106**(47): p. 20051-6.
30. Volpicelli-Daley, L.A., K.C. Luk, and V.M. Lee, *Addition of exogenous α-synuclein preformed fibrils to primary neuronal cultures to seed recruitment of endogenous α-synuclein to Lewy body and Lewy neurite-like aggregates.* Nat Protoc, 2014. **9**(9): p. 2135-46.
31. Gray, S.J., et al., *Optimizing promoters for recombinant adeno-associated virus-mediated gene expression in the peripheral and central nervous system using self-complementary vectors.* Hum Gene Ther, 2011. **22**(9): p. 1143-53.
32. Vardaman, D., 3rd, et al., *Development of a Spectral Flow Cytometry Analysis Pipeline for High-Dimensional Immune Cell Characterization.* bioRxiv, 2024.
33. Braak, H., et al., *Staging of brain pathology related to sporadic Parkinson's disease.* Neurobiol Aging, 2003. **24**(2): p. 197-211.
34. DeKosky, S.T. and S.W. Scheff, *Synapse loss in frontal cortex biopsies in Alzheimer's disease: correlation with cognitive severity.* Ann Neurol, 1990. **27**(5): p. 457-64.
35. Greffard, S., et al., *Motor score of the Unified Parkinson Disease Rating Scale as a good predictor of Lewy body-associated neuronal loss in the substantia nigra.* Arch Neurol, 2006. **63**(4): p. 584-8.
36. Selkoe, D.J., *Alzheimer's disease is a synaptic failure.* Science, 2002. **298**(5594): p. 789-91.

37. Harms, A.S., et al., *Peripheral monocyte entry is required for alpha-Synuclein induced inflammation and Neurodegeneration in a model of Parkinson disease.* Exp Neurol, 2018. **300**: p. 179-187.
38. Heneka, M.T., et al., *NLRP3 is activated in Alzheimer's disease and contributes to pathology in APP/PS1 mice.* Nature, 2013. **493**(7434): p. 674-8.
39. Maphis, N., et al., *Reactive microglia drive tau pathology and contribute to the spreading of pathological tau in the brain.* Brain, 2015. **138**(Pt 6): p. 1738-55.
40. Deczkowska, A., et al., *Disease-Associated Microglia: A Universal Immune Sensor of Neurodegeneration.* Cell, 2018. **173**(5): p. 1073-1081.
41. Krasemann, S., et al., *The TREM2-APOE Pathway Drives the Transcriptional Phenotype of Dysfunctional Microglia in Neurodegenerative Diseases.* Immunity, 2017. **47**(3): p. 566-581.e9.
42. Traag, V.A., L. Waltman, and N.J. van Eck, *From Louvain to Leiden: guaranteeing well-connected communities.* Sci Rep, 2019. **9**(1): p. 5233.
43. Ferretti, M.T., et al., *T-cell brain infiltration and immature antigen-presenting cells in transgenic models of Alzheimer's disease-like cerebral amyloidosis.* Brain Behav Immun, 2016. **54**: p. 211-225.
44. Mucke, L., et al., *High-level neuronal expression of abeta 1-42 in wild-type human amyloid protein precursor transgenic mice: synaptotoxicity without plaque formation.* J Neurosci, 2000. **20**(11): p. 4050-8.
45. Wright, A.L., et al., *Neuroinflammation and neuronal loss precede Aβ plaque deposition in the hAPP-J20 mouse model of Alzheimer's disease.* PLoS One, 2013. **8**(4): p. e59586.
46. Saganich, M.J., et al., *Deficits in synaptic transmission and learning in amyloid precursor protein (APP) transgenic mice require C-terminal cleavage of APP.* J Neurosci, 2006. **26**(52): p. 13428-36.
47. Oddo, S., et al., *Triple-transgenic model of Alzheimer's disease with plaques and tangles: intracellular Abeta and synaptic dysfunction.* Neuron, 2003. **39**(3): p. 409-21.
48. Lewis, J., et al., *Enhanced neurofibrillary degeneration in transgenic mice expressing mutant tau and APP.* Science, 2001. **293**(5534): p. 1487-91.
49. Shipton, O.A., et al., *Tau protein is required for amyloid {beta}-induced impairment of hippocampal long-term potentiation.* J Neurosci, 2011. **31**(5): p. 1688-92.
50. Giasson, B.I., et al., *Initiation and synergistic fibrillization of tau and alpha-synuclein.* Science, 2003. **300**(5619): p. 636-40.
51. Andorfer, C., et al., *Hyperphosphorylation and aggregation of tau in mice expressing normal human tau isoforms.* J Neurochem, 2003. **86**(3): p. 582-90.
52. Duff, K., et al., *Increased amyloid-beta42(43) in brains of mice expressing mutant presenilin 1.* Nature, 1996. **383**(6602): p. 710-3.
53. Lewis, J., et al., *Neurofibrillary tangles, amyotrophy and progressive motor disturbance in mice expressing mutant (P301L) tau protein.* Nat Genet, 2000. **25**(4): p. 402-5.
54. Decressac, M., et al., *Progressive neurodegenerative and behavioural changes induced by AAV-mediated overexpression of α-synuclein in midbrain dopamine neurons.* Neurobiol Dis, 2012. **45**(3): p. 939-53.
55. Elabi, O., et al., *Human α-synuclein overexpression in a mouse model of Parkinson's disease leads to vascular pathology, blood brain barrier leakage and pericyte activation.* Sci Rep, 2021. **11**(1): p. 1120.

56. Karikari, A.A., et al., *Neurodegeneration by α-synuclein-specific T cells in AAV-A53T-α-synuclein Parkinson's disease mice.* Brain Behav Immun, 2022. **101**: p. 194-210.
57. Schonhoff, A.M., et al., *Border-associated macrophages mediate the neuroinflammatory response in an alpha-synuclein model of Parkinson disease.* Nat Commun, 2023. **14**(1): p. 3754.
58. Gómez-Benito, M., et al., *Modeling Parkinson's Disease With the Alpha-Synuclein Protein.* Front Pharmacol, 2020. **11**: p. 356.
59. Pinto-Costa, R., et al., *Overexpression-Induced α-Synuclein Brain Spreading.* Neurotherapeutics, 2023. **20**(1): p. 83-96.
60. Cheng, H.C., C.M. Ulane, and R.E. Burke, *Clinical progression in Parkinson disease and the neurobiology of axons.* Ann Neurol, 2010. **67**(6): p. 715-25.
61. Gómez-Isla, T., et al., *Neuronal loss correlates with but exceeds neurofibrillary tangles in Alzheimer's disease.* Ann Neurol, 1997. **41**(1): p. 17-24.
62. Gómez-Isla, T., et al., *Profound loss of layer II entorhinal cortex neurons occurs in very mild Alzheimer's disease.* J Neurosci, 1996. **16**(14): p. 4491-500.
63. Masliah, E., et al., *Synaptic and neuritic alterations during the progression of Alzheimer's disease.* Neurosci Lett, 1994. **174**(1): p. 67-72.
64. Chu, Y., et al., *Nigrostriatal tau pathology in parkinsonism and Parkinson's disease.* Brain, 2024. **147**(2): p. 444-457.
65. Irwin, D.J., V.M. Lee, and J.Q. Trojanowski, *Parkinson's disease dementia: convergence of α-synuclein, tau and amyloid-β pathologies.* Nat Rev Neurosci, 2013. **14**(9): p. 626-36.
66. Lim, A., et al., *Clinico-neuropathological correlation of Alzheimer's disease in a community-based case series.* J Am Geriatr Soc, 1999. **47**(5): p. 564-9.
67. Lashley, T., et al., *Cortical alpha-synuclein load is associated with amyloid-beta plaque burden in a subset of Parkinson's disease patients.* Acta Neuropathol, 2008. **115**(4): p. 417-25.
68. Nelson, P.T., H. Braak, and W.R. Markesbery, *Neuropathology and cognitive impairment in Alzheimer disease: a complex but coherent relationship.* J Neuropathol Exp Neurol, 2009. **68**(1): p. 1-14.
69. Wetering, J.V., et al., *Neuroinflammation is associated with Alzheimer's disease co-pathology in dementia with Lewy bodies.* Acta Neuropathol Commun, 2024. **12**(1): p. 73.
70. Gu, H., et al., *Lymphocyte Activation Gene 3 (Lag3) Contributes to α-Synucleinopathy in α-Synuclein Transgenic Mice.* Front Cell Neurosci, 2021. **15**: p. 656426.
71. Chen, Y. and Y. Yu, *Tau and neuroinflammation in Alzheimer's disease: interplay mechanisms and clinical translation.* J Neuroinflammation, 2023. **20**(1): p. 165.
72. Hansen, D.V., J.E. Hanson, and M. Sheng, *Microglia in Alzheimer's disease.* J Cell Biol, 2018. **217**(2): p. 459-472.
73. Heneka, M.T., et al., *Neuroinflammation in Alzheimer's disease.* Lancet Neurol, 2015. **14**(4): p. 388-405.
74. Imamura, K., et al., *Distribution of major histocompatibility complex class II-positive microglia and cytokine profile of Parkinson's disease brains.* Acta Neuropathol, 2003. **106**(6): p. 518-26.
75. Zeng, J., et al., *T cell infiltration mediates neurodegeneration and cognitive decline in Alzheimer's disease.* Neurobiol Dis, 2024. **193**: p. 106461.
76. Grabert, K., et al., *Microglial brain region-dependent diversity and selective regional sensitivities to aging.* Nat Neurosci, 2016. **19**(3): p. 504-16.

77. Streit, W.J., et al., *Dystrophic microglia in the aging human brain.* Glia, 2004. **45**(2): p. 208-12.
78. Gruden, M.A., et al., *Immunoprotection against toxic biomarkers is retained during Parkinson's disease progression.* J Neuroimmunol, 2011. **233**(1-2): p. 221-7.
79. Kustrimovic, N., et al., *Parkinson's disease patients have a complex phenotypic and functional Th1 bias: cross-sectional studies of CD4+ Th1/Th2/T17 and Treg in drug-naïve and drug-treated patients.* J Neuroinflammation, 2018. **15**(1): p. 205.
80. Rocha, N.P., et al., *Reduced Activated T Lymphocytes (CD4+CD25+) and Plasma Levels of Cytokines in Parkinson's Disease.* Mol Neurobiol, 2018. **55**(2): p. 1488-1497.
81. Reynolds, A.D., et al., *Regulatory T cells attenuate Th17 cell-mediated nigrostriatal dopaminergic neurodegeneration in a model of Parkinson's disease.* J Immunol, 2010. **184**(5): p. 2261-71.
82. Smolders, J., et al., *Characteristics of differentiated CD8(+) and CD4 (+) T cells present in the human brain.* Acta Neuropathol, 2013. **126**(4): p. 525-35.
83. Masliah, E., et al., *Effects of alpha-synuclein immunization in a mouse model of Parkinson's disease.* Neuron, 2005. **46**(6): p. 857-68.
84. Masliah, E., et al., *Passive immunization reduces behavioral and neuropathological deficits in an alpha-synuclein transgenic model of Lewy body disease.* PLoS One, 2011. **6**(4): p. e19338.